THE ASTROPHYSICAL JOURNAL, 201:661–694, 1975 November 1

GAS FLOW IN CATACLYSMIC VARIABLE STARS*

BRIAN P. FLANNERY
Lick Observatory, Board of Studies in Astronomy and Astrophysics,
University of California, Santa Cruz
Received 1975 February 14; revised 1975 April 21

ABSTRACT

A numerical hydrodynamic scheme, applicable to gas flow in binary stars, is presented which incorporates the effects of pressure and gravitational forces, radiative cooling, and shock formation. The method is used to study gas flow originating from Roche lobe overflow through the inner Lagrangian point, L_1, in a binary star modeled to resemble the dwarf nova Z Cam. Three mass transfer rates, $3 \times (10^{-9}, 10^{-8}, 10^{-7})\ M_\odot\ \text{year}^{-1}$, are followed for a total time of 1.50 binary orbital periods. The calculations indicate that rapid energy dissipation, via radiative cooling in a shock front formed between the stream from L_1 and the returning gas which has circuited the star, quickly transforms the flow into a stream-ring configuration. An optically thick, confined shock forms at the intersection of the stream and ring. At a transfer rate of $3 \times 10^{-9}\ M_\odot\ \text{year}^{-1}$ the shock's location, temperature (23,000 K at maximum), and energy release (8×10^{32} ergs s^{-1}) are in substantial agreement with observations of Z Cam, and confirm the major elements of the "hot spot" model proposed to account for observations of cataclysmic variable stars.

Subject headings: binaries — dwarf novae — hydrodynamics — mass loss

I. INTRODUCTION

Observations reveal features interpretable as arising in gas streams in many types of close double stars (Batten 1970). While theoretical studies provide a basic framework which explains the existence of streams in terms of mass transfer driven by evolutionary expansion, details of the actual mass transfer are not considered in such studies (see the review articles by Plavec 1968 and Paczynski 1971). Until recently studies of streams were based on particle trajectories in the restricted three body approximation. The results of Kuiper (1941), Kopal (1956), Gould (1957, 1959), and Kruszewski (1964), among others, indicated some basic properties such as velocities and directions of flow which might be expected in gas streams. However, the problem is necessarily hydrodynamic in character because of the short mean free paths expected and because the trajectories collide with one another and the stellar surfaces. As a first attempt to introduce hydrodynamic considerations, Prendergast (1960) developed a solution for streamlines in the orbital plane of a generalized binary, subject to several constraining assumptions. In particular, velocity components at right angles to Roche equipotential surfaces were assumed small, and pressure terms were neglected. Furthermore, no specific boundary conditions were imposed, so the results were again only indicative of likely flow directions and magnitudes in various regions. Bierman (1971), using the method of characteristics, produced flow patterns in the orbital plane for supersonic mass loss from the surface of a binary component filling its Roche lobe. The gas was assumed to maintain constant thickness out of the plane. Although, as expected, shock formation occurred near the mass-receiving star (invalidating the use of characteristics), his results suggested ring formation around that star. However, it is unlikely that such supersonic mass transfer is normal or that it could be confined to the orbital plane. In neither Prendergast's nor Bierman's investigations could the effect of a stellar atmosphere be included. Recently, Prendergast and Taam (1974) presented a method for calculating hydrodynamic flow allowing for shocks, pressure terms, radiative cooling, and approximately incorporating the presence of a stellar atmosphere. Their scheme was applied to study gas flow in a system of $4\ M_\odot$, $2\overset{d}{.}5$ period, and 2:1 mass ratio modeled to resemble U Cep. They considered mass transfer through the inner Lagrangian point, L_1, for a variety of rotation rates for the component transferring mass. After following the flow for roughly one orbital period, they found that the bulk of the transferred gas was absorbed immediately by the companion, a small fraction of the gas managed to circuit around the star and was swept back into the main stream from L_1, and a smaller fraction of the gas escaped the stellar Roche lobes entirely. Although direct observational comparisons could not be simply facilitated, some correspondences were found. Additional details of their numerical method can be found in Sanders and Prendergast (1974).

This paper presents an independently developed, general method for simulating gas flow in binary stars and applies the method to examine mass transfer in a system resembling the short-period cataclysmic variable (CV) stars: novae, recurrent novae, dwarf novae, and nova-like variables. In spite of an enormous range in eruptive activity, these stars are basically similarly

* *Lick Observatory Bulletin*, No. 698.

constituted binary stars (see the review article by Kraft 1963). The dominant observational properties of these stars at minimum light arise from gaseous features; frequently no obviously stellar features are visible. While each of the well studied CV stars displays unique peculiarities, as a class their gaseous components seem very similar. The common binary model consists of a late type, red star filling its Roche lobe and transferring gas into a ring or disk surrounding a hot, blue star, probably a white dwarf. Broad, occasionally double emission lines of H, He I, Ca II (and He II in old novae) which dominate the spectra arise in the disk, while variable photometric flickering is attributed to luminosity originating in the gaseous stream and disk. This model has been elaborated independently by Warner and Nather (1971) and Krzemiński and Smak (1971) who suggest that a significant fraction of the observed light originates in a shock front or "hot spot" where the disk and stream intersect. This feature accounts for many photometric peculiarities such as eclipses which lag spectroscopic conjunction and vary in phase, and a hump with increased flickering in the light curve preceding eclipse. Although observationally few in number and apparently faint at minimum light, CV stars are associated with several astrophysically interesting problems in which mass transfer plays an important role. Among these are problems relating to the outburst mechanism and the wide range of activity in such seemingly similar systems. The evolutionary status of these stars is unknown; it is not even clear whether the progression in periods from 10 hours to 1 hour represents an evolutionary sequence. There is also a strong possibility that gravitational radiation, by removing orbital angular momentum, provides the stimulus for mass transfer and thereby controls the evolution of CV stars. The review article of Faulkner (1974) provides references and further details regarding theoretical aspects of CV stars, while the reviews by Kraft (1963) and Mumford (1967) summarize observations of CV stars.

In outline this paper proceeds as follows. The differential equations governing gas flow in binary stars are formulated in the next section, and a method for their numerical solution is described in § III. Calculations of mass transfer in a system parametrized to resemble the dwarf nova Z Cam, one of the most studied CV stars, are presented in § IV. In § V some of the hydrodynamic results are compared with particle trajectory models for the hot spot. Section VI summarizes results of both the hydrodynamic and particle trajectory models and discusses their implications with regard to mass transfer in general and CV stars and the hot spot model in particular. Conclusions are presented in § VII.

II. FORMULATION OF THE PROBLEM

The basic form of the dominant gravitational potential suggests the utility of formulating the binary gas-flow problem in cylindrical coordinates in a frame of reference rotating at the binary orbital frequency ω. In these coordinates, with the z axis perpendicular to the orbital plane, the hydrodynamic equations in component form are

$$\frac{\partial \rho}{\partial t} = -\nabla \cdot \rho \bar{v}\,, \tag{1}$$

$$\frac{\partial v_z}{\partial t} = -\bar{v} \cdot \nabla v_z - \frac{\partial \psi}{\partial z} - \frac{1}{\rho}\frac{\partial P}{\partial z}\,, \tag{2}$$

$$\frac{\partial v_r}{\partial t} = -\bar{v} \cdot \nabla v_r - \frac{\partial \psi}{\partial r} - \frac{1}{\rho}\frac{\partial P}{\partial r} + v_\theta\left(2\omega + \frac{v_\theta}{r}\right), \tag{3}$$

$$\frac{\partial v_\theta}{\partial t} = -\bar{v} \cdot \nabla v_\theta - \frac{\partial \psi}{r\partial \theta} - \frac{1}{\rho}\frac{\partial P}{r\partial \theta} - v_r\left(2\omega + \frac{v_\theta}{r}\right), \tag{4}$$

$$\frac{\partial(\psi + v^2/2 + \epsilon)}{\partial t} = -\bar{v} \cdot \nabla(\psi + v^2/2 + \epsilon) - \frac{1}{\rho}\nabla \cdot P\bar{v} + q. \tag{5}$$

Each of the variables are functions of the coordinates r, θ, z, and time t: ρ, P, ϵ are the gaseous density pressure and internal energy (per gram); v_r, v_θ, v_z are the scalar velocity components (terms arising from the operation of the gradient on the basis vectors are explicitly written in eqs. [2]–[4]); q is a radiative loss term; and ψ is the Roche potential. The Roche potential is

$$\psi = \frac{-GM}{a}\left[\mu/r_1 + (1-\mu)/r_2 + d^2/2\right], \tag{6}$$

in which G is the gravitational constant, M and a are the total binary system mass and separation, μ is the mass fraction in star 1, r_1 (r_2) is the distance in units of a from star 1 (2), and d is the perpendicular distance, again in units of a, from the binary rotation axis. Use of the Roche potential assumes (1) the gravitational potential of each star can be approximated as though each star's mass were concentrated at its center, and (2) the binary orbit is circular, approximations which are particularly valid in CV stars. The star receiving mass is taken as coordinate origin with $\theta = 0$ directed away from the star transferring mass. Throughout the paper the star receiving mass is referred to as the white dwarf or blue star and is designated by subscript 1; the mass fraction μ refers to the mass fraction of this star, i.e., $M_1 = \mu M$. The red star (star 2) has mass fraction $1 - \mu$.

A numerical solution of these three-dimensional, time-dependent equations is not feasible without the introduction of simplifications. Perfect gas laws are used, and a constant ionization with a mean atomic weight of one-half is assumed. Therefore, the gas pressure and internal energy are

$$P = 2\rho RT\,, \tag{7}$$

$$\epsilon = \frac{3}{2}\frac{P}{\rho}\,, \tag{8}$$

with R the gas constant. Also, a simple model for the

gas behavior out of the orbital plane is adopted which circumvents numerous difficulties and uncertainties. Effects of convection, exterior radiation fields, and variable energy release with z all enter into a discussion of the gaseous z distribution. However, for relatively small velocities out of the plane, motions in z should be damped quickly. As a simple approximation which at least allows a rough inclusion of the third spatial dimension, hydrostatic equilibrium and isothermality in z are assumed. It is also assumed that the flow thickness out of the plane is much smaller than the distance to either star; this assumption can be verified during the calculations. The potential may then be expanded with respect to z in Taylor series; one finds

$$\psi(r, \theta, z) \approx \psi(r, \theta, 0) + A(r, \theta)\frac{z^2}{2}, \tag{9}$$

$$A(r, \theta) = \frac{GM_1}{r_1^3} + \frac{GM_2}{r_2^3}. \tag{10}$$

Solution of equation (2) then yields the density distribution with z,

$$\rho(r, \theta, z) = \rho(r, \theta, 0) \exp\left[-(z/L)^2\right], \tag{11}$$

with the disk semithickness L given by

$$L = (4RT/A)^{1/2}. \tag{12}$$

Equations (1–5), with ψ and ρ replaced by equations (9) and (11), can be integrated over z to find two dimensional equations for the flow variables v_r, v_θ, the column density σ, and the specific energy e, now only functions of r, θ, and time. With the definitions

$$T^* = 2RT, \tag{13}$$

$$\sigma = \int_{-\infty}^{\infty} \rho(r, \theta, z)dz, \tag{14}$$

$$e = \psi + v^2/2 + 2T^*, \tag{15}$$

the flow equations become

$$\frac{\partial \sigma}{\partial t} = -\nabla \cdot \sigma \bar{v}, \tag{16}$$

$$\frac{\partial v_r}{\partial t} = -\bar{v}\cdot\nabla v_r - \frac{\partial \psi}{\partial r} - \frac{T^*}{2A}\frac{\partial A}{\partial r} - \frac{1}{\sigma}\frac{\partial \sigma T^*}{\partial r} + v_\theta\left(2\omega + \frac{v_\theta}{r}\right), \tag{17}$$

$$\frac{\partial v_\theta}{\partial t} = -\bar{v}\cdot\nabla v_\theta - \frac{\partial \psi}{r\partial \theta} - \frac{T^*}{2A}\frac{\partial A}{r\partial \theta} - \frac{1}{\sigma}\frac{\partial \sigma T^*}{r\partial \theta} - v_r\left(2\omega + \frac{v_\theta}{r}\right), \tag{18}$$

$$\frac{\partial e}{\partial t} = -\bar{v}\cdot\nabla e - \frac{1}{\sigma}\nabla\cdot\sigma T^*\bar{v} + Q. \tag{19}$$

The radiative loss term, Q, is evaluated for the case of optically thick blackbody radiation, with only losses through the disk surfaces considered; therefore,

$$Q = 2\sigma_{sb}T^4/\sigma, \tag{20}$$

where σ_{sb} is the Stefan-Boltzmann constant (the factor of 2 allows for radiation from both disk surfaces). Although the actual optical depth through the disk of CV stars is unknown, it seems likely that the disks are optically thick. A rough estimate (based on Rosseland mean opacities) shows that to achieve an optical depth $\tau \approx 2$ through the disk requires the following conditions: at 10^4 K, $\sigma \approx 0.2$ (g cm^{-2}); at high temperatures where electron scattering is important, $\sigma \approx 6$; and below about 8×10^3 K large column densities are necessary, say $\sigma \approx 20$. While at low temperatures the disk may not be optically thick unless dust is present, by that point thermal effects have little influence on the dynamic flow. For a typical CV star with a disk area of 10^{21} cm^2 and a mass transfer rate conservatively estimated at 10^{16} g s^{-1} only a few days' accumulation of gas results in an optically thick disk (if the gas is retained in the disk). For this cooling rate, equation (20), the cooling time is

$$t_c = 2.9\sigma/(T/10^4\ \mathrm{K})^3 \text{ seconds}. \tag{21}$$

Note that if the total opacity were dominated by scattering, s, rather than true absorption, k (as can occur at very high or low temperatures), then the cooling rate would be reduced by a factor $(k/s)^{1/2}$. For this problem such conditions would be most important at high temperatures, where the net effect would be, roughly, to augment the equilibrium temperature by a factor $(s/k)^{1/8}$, i.e. 33 percent for $s/k = 10$.

In this study an initial mass transfer rate of $3 \times 10^{-8}\ M_\odot$ year^{-1} (2×10^{18} g s^{-1}) is used to develop an optically thick disk rapidly. Optically thin cooling would alter few if any of the results described later since cooling rates are very rapid in this problem even for optically thin cooling. The case of optically thin cooling is discussed in the Appendix.

The final two-dimensional equations derived here are similar to those obtained by Prendergast and Taam. However, they cooled the gas in an optically thin approximation, appropriate for their system. In either case cooling times often are far shorter than the dynamically determined time steps used in the numerical solution. They avoided the obvious difficulties associated with too rapid cooling by assuming that a minimum temperature of 10^4 K would be maintained by the ambient radiation field of the two hot, luminous stars comprising the binary. Although the spectra of CV stars indicate the presence of an ionized gas, it is not certain that complete ionization of the entire disk can be maintained. The blue star's ability to irradiate the gas with ionizing photons is unclear for geometrical, as well as energetic, reasons, while the red star could not generate such high temperatures. Therefore the gas is allowed to cool to a minimum temperature of 10 K, and only mechanical heating is considered.

III. THE NUMERICAL METHOD

This section discusses solution of the differential equations (16)–(19) by difference equations in a cylindrical Eulerian grid. In overview the method utilizes a Lagrangian step, during which the changes and movement of the gas in each cell at the initiation of a time step are followed, and a mixing step, during which the final mass, momentum, and energy of this gas at the termination of the time step are distributed into the Eulerian cells which the gas entered. From the accumulated mass, momentum, and energy in each cell at the end of the time step, the flow variables σ, v_r, v_θ, and e are directly obtainable. For stability in calculating the flow a time step dt is chosen such that the gas in any cell travels at most its own length (in r or θ) during the time step, roughly a Courant condition. However, this procedure is forced by the limited grid resolution to regard any gas entering a cell as uniformly distributed through the cell, regardless of how far the gas actually penetrated. To avoid modifying the energy or angular momentum of the gas by this unphysical mixing requires applying corrections to an otherwise straightforward process.

a) The Basic Numerical Method

Together with the flow variables, also defined in each cell are the invariant potential representing quantities ψ and A, and a set of variables M, P_r, P_θ, and E which accumulate the influx of mass, momentum, and energy entering a cell during a time step. Consider the Lagrangian step following the motion of gas of mass $m = \sigma dA$ originally in a cell at r, θ of dimensions dr, $d\theta$, and area dA. Changes in the velocity and energy of this gas are derived from their convective derivatives which are numerically evaluated. These are obtained directly from equations (17)–(19) by transposition of the $\bar{v}\cdot\nabla(v_r, v_\theta,$ and $e)$ terms to the left-hand side of the equations since

$$\frac{Df}{Dt} = \frac{\partial f}{\partial t} + \bar{v}\cdot\nabla f\,. \tag{22}$$

Time derivatives are explicitly evaluated at time t only, and gradients are evaluated as differences of quantities in cells at $r \pm dr$ and $\theta \pm d\theta$. The radiative loss term in equation (19) is temporarily deleted for inclusion at a later phase of the calculation.

From the difference equations quantities v_r', v_θ', and e' characterize the gas, still of mass m, at time $t + dt$, but with its center of mass now at $\bar{r}' = \bar{r} + \bar{v}dt$, and $\psi' = \psi + \bar{v}\cdot\nabla\psi dt$. The fraction by mass of the gas leaving the original cell through the boundary in r or θ during the time step is

$$f_r = |v_r' dt/dr|\,, \tag{23}$$

$$f_\theta = |v_\theta' dt/r d\theta|\,. \tag{24}$$

These fractions determine the mass of gas entering each of at most four influenced cells. For example, the mass remaining in the original cell is $(1 - f_r)(1 - f_\theta)m$. Similarly, the momentum mv_r', mv_θ' and energy me' are fractionally partitioned, but at this point the fractions are slightly modified to avoid altering the specific angular momentum or energy of the mixed gas. The correction factors are discussed in the next subsection. After the transport process has operated on every cell in the grid, the cumulative variables M, P_r, P_θ, and E represent the gas at time $t + dt$.

From these variables the column density and velocity are directly obtained: $\sigma = M/dA$, $v_r = P_r/M$, $v_\theta = P_\theta/M$. To find e (and therefore T^*) requires inclusion of the earlier neglected radiative losses. Without losses

$$e'' = E/M\,, \tag{25}$$

$$T^{*\prime\prime} = \tfrac{1}{2}(e'' - \psi - v^2/2)\,. \tag{26}$$

The cooling rate is applied to these variables for a time dt to find

$$T^* = T^{*\prime\prime}\left(1 + \frac{3\sigma_{sb}T^{*\prime\prime 3}dt}{16R^4\sigma}\right)^{-1/3}, \tag{27}$$

$$e = \psi + v^2/2 + 2T^*\,. \tag{28}$$

Application of the radiative cooling at the end of the time step allows for radiation of thermal energy acquired during the time step, which can be considerable.

b) Corrections Applied in the Mixing Step

As explained below, if the momentum and energy were fractionally partitioned in the same manner used to distribute the mass, the mixing process would alter the specific energy and angular momentum (with respect to the blue star in the nonrotating frame of reference) of the artificially transported gas in a fashion that can seriously affect the entire flow. Therefore, corrections are applied such that these quantities are unaltered in mixing. Note that the corrections do not cause the energy and angular momentum to become conserved quantities; they are not. Rather, they allow variations to be generated solely by the differential equations, not by the unphysical mixing required by the Eulerian grid.

The specific angular momentum of the gas is

$$j = r(v_\theta + \omega r)\,; \tag{29}$$

the second term accounts for the rotating frame of reference. The presence of pressure terms and a second center of gravitational force causes the angular momentum with respect to the blue star to be variable. However, near the blue star j will be nearly constant, as can be verified by particle trajectory calculations. Since the variables e and j are dynamically the two most important determinants of the global flow, neither should be varied arbitrarily. A subscript c is used to designate variables in one of the cells into which gas is mixed from its position at r', ψ' as in the previous subsection. Let f_c be the fraction by mass of the gas at r' entering cell c. In order to conserve angular momentum, when the momentum mv' is distributed

into cell c, the increment added to the cumulative variable $P_{\theta c}$ is

$$dP_{\theta c} = f_c m[r' v_\theta' + \omega(r'^2 - r_c^2)]/r_c \,. \quad (30)$$

Similarly since the potential component of the energy e' varies by $\Delta\psi = \psi' - \psi_c$, the nonpotential components must jointly change by $-\Delta\psi$. The mixed value of the angular velocity, $v_{\theta c}$, is already known from the previous correction. The energy invariance can be accomplished by modifying the increment to P_{rc} such that

$$dP_{rc} = f_c m v_r' \left(\frac{e' - \psi_c - v_c^2/2}{e' - \psi' - v'^2/2}\right)^{1/2} . \quad (31)$$

Implicitly, the same factor modifying mv_r' acts on the thermal content of the mixing gas; this has little effect on the energy balance since the flow is highly supersonic throughout the grid. The numerator in equation (31) can become negative when a turning point in radial velocity straddles r', r_c; in that case the gas is reflected in radial velocity.

Failure to include these corrections results in unduly increasing the kinetic energy of the gas mixing through $\Delta\psi < 0$ (outward in radius), and removing, not transferring, angular momentum from gas traveling inward in radius during mixing. If sufficient thermal energy is available to provide the kinetic energy increase the subtraction of equation (26) balances the spurious increase in kinetic energy at the expense of the gaseous thermal energy. However, the highly supersonic nature of the flow is such that the erroneous increase in kinetic energy often produces a negative solution for the temperature. In that case setting the temperature to some minimum value compounds the error by adding even more energy to the gas. Calculations of mass transfer without including either correction indicated that nearly 60 percent of the transferred gas achieved sufficient velocity to escape the stellar Roche lobe during its first pass around the star. This is a consequence of the fact that the potential drop between L_1 and initial closest approach of the gas to the white dwarf was nearly 40 times greater than the potential difference between the outer Lagrangian points and L_1. Thus, failure to conserve energy by only 2–3 percent can produce significant mass loss. Calculations performed with only an energy-conserving correction applied equally to v_r and v_θ showed that no mass loss occurred, and a disk rapidly formed. However the disk soon collapsed inside the grid's inner boundary as angular momentum disappeared from gas flowing toward the center. The necessity of applying these corrections is primarily a consequence of the large variation in potential and radius spanned by the gas flow in CV stars.

c) *Zoning and Boundary Conditions*

For low-velocity flow through L_1, unless energy is added or preferentially transferred to some part of the flow, the gas will be confined to the region bounded by the Roche equipotential through L_1. Therefore, a grid is defined which basically covers the region accessible to the gas flow. Also, particle trajectories indicate that the stream from L_1 will pass within about 0.06 in r/a from the origin for a mass ratio of 0.60 as used in the calculations for Z Cam (see Fig. 4 of Flannery 1975). A typical white dwarf of 10^9 cm radius in a CV binary of 10^{11} cm separation is comfortably avoided by particle flow, but, to follow the flow, the grid must extend deep into the potential well surrounding the white dwarf.

An important feature of the numerical method is an allowance for variable cell sizes. The increment in radius is 0.01 in r/a over most of the grid, but logarithmic increments of $dr/r \approx 0.06$ are employed near the origin to maintain high accuracy in replacing $\nabla\psi$ by a differenced potential across neighboring cells. Small angular spacing, $d\theta < 1°$, is used near L_1 to resolve the influx of gas; moderate spacing, $d\theta \approx 2°$, prevails over most of the grid; and larger spacing, $3°6 < d\theta < 36°$, is necessary deep in the potential where prohibitively short time steps might result if gas entered the cells. The overall division of the grid is apparent in Figure 2 where only every other cell in r and θ is plotted; the entire grid contains roughly 8000 cells distributed among eight zones.

Boundary conditions are fortunately simple. Except near L_1 where gas is injected at a thermal velocity, the outer boundary is a vacuum. Gas leaving the grid through the outer boundary is simply tabulated but disappears from further consideration. In the calculations only a small amount of gas ever leaves the grid. While cells are defined to 0.01 in r/a, very little angular momentum transfer occurs during the time the flow could be followed. Consequently no gas penetrated deep enough to have interacted directly with the white dwarf.

d) *Problems and Sources of Error*

The major uncertainty in results derived from this method arises from an artificial spreading induced by mixing gas through an entire cell when its velocity would have permitted only partial penetration. Concurrent with the broadening is an artificial viscosity which depends on (1) the cell size, (2) the orientation of the velocity vector with respect to the cell boundary, and (3) the time step. Obviously, if cell sizes could be maintained small with respect to density gradients, the problem could be made negligible. However, in binary gas flow where virtually stream–vacuum interfaces can occur, this is impossible. Matching of cell orientation with respect to streamlines minimizes the problem, another reason for the choice of cylindrical coordinates.

The temperature determination is liable to two sources of error. First, it is derived from a subtraction of two much larger quantities. Second, the cooling time can be much shorter than the time step. The dynamic flow is not appreciably altered by either error since the errors are greatest where the temperature and density are smallest.

Several more obvious sources of error are in fact

not serious. Although pressure gradients may be in error near stream–vacuum interfaces, the predominating gravitational force is nowhere in error from its true value by more than 0.25 percent. Since the gas travels one cell length only in the center where velocities rapidly become nearly circular, use of a constant force during the Lagrangian step is adequate. Rapid equilibration of the flow reduces errors caused by using explicit time derivatives. Finally, the energy conservation correction eliminates possible introduction of energy by the differenced force evaluation. Except for radiative losses and the boundary influx of energy, energy is conserved across the grid.

The entire computational procedure was tested by directing a uniform stream against a wedge for several Mach numbers and inclinations of stream to wedge. Constant thickness was assumed, and no radiative losses were allowed. The oblique shocks produced in this problem can be found analytically by using the Rankine-Hugoniot jump conditions. Calculations performed both with and without an explicit artificial viscosity term produce reasonably accurate solutions. In both cases a shock front forms at the expected angle of inclination, and postshock variables match their expected values on average. Downstream from the shock the flow develops a cell structure, much larger than the grid cell size, across which variables fluctuate by 10 and 20 percent with and without the viscous term, respectively. The cell structure seems related to the "ragged" shock front which forms since the grid cells cannot smoothly represent the inclined shock. Without the viscous term a small, variable velocity component perpendicular to the wedge is present which enhances the cell structure, while the velocity is parallel to the wedge with the viscous term. The results of this test seemed satisfactory enough to avoid intentionally adding an explicit artificial viscosity term in the differential equations.

IV. CALCULATIONS OF MASS TRANSFER

This section describes the results of calculations of mass transfer in a binary star parametrized to resemble the dwarf nova Z Cam. The results should not be construed as a complete, exact model for gaseous flow in this particular system, because: first, the flow could only be followed for about one binary period; second, the ultimately derived temperature distribution cannot be converted simply into integrated radiation for observational comparisons; and third, the assumptions used to derive the temperature probably produce factor of two accuracy at best. Nonetheless, it seemed advisable to model a specific, well studied star so that correlations with observations might be attempted.

Z Cam is one of the few CV stars for which reliable estimates of system parameters are available. Spectroscopically, Z Cam is a double-lined binary exhibiting both disk emission lines and G star absorption lines (Kraft *et al.* 1969). The photometric light curve displays large-scale flickering and is nonrepetitive from cycle to cycle. Eclipses are not visible, or are at best transient and partial, but the hump characteristic of CV stars is presented from phase 0.6P to 0.15P, peaking at about phase 0.87P from spectroscopic conjunction. In spite of an absence of eclipses, other considerations provide a reliable estimate of the orbital inclination. Robinson (1973*a*) suggests that the red and blue components have masses of 1.0 and 1.3 $M_\odot$, respectively. An estimate of the mass transfer rate in Z Cam of $3 \times 10^{-9}\ M_\odot\ \text{year}^{-1}$ (a lower limit) was made by Robinson (1973*b*). This estimate assumes that the red star produces 1 solar luminosity, in accordance with its mass and spectral type; that the transferred mass liberates the entire energy made available from the potential drop between L_1 and the hot spot; and that the energy is liberated at the hot spot which he estimates to produce 25 percent as much luminosity as the red star. Unfortunately the lack of eclipses in Z Cam reduces the known information concerning its hot spot as compared with such systems as U Gem (Krzemiński 1965, Warner and Nather 1971), WZ Sge (Krzemiński and Smak 1971; Warner and Nather 1972*a*), or VV Pup (Warner and Nather 1972*b*). However, the masses and luminosities of these systems are not nearly as well known as for Z Cam. For the calculations the model binary used has a period of 2.5×10^4 s, a total mass of 2.4 $M_\odot$ (with 60% in the white dwarf), and a separation of 1.72×10^{11} cm.

The integrations cover a total physical time of 1.50P (binary orbital periods) during which three different mass transfer rates are used. The first period is calculated with a transfer rate of $3 \times 10^{-8}\ M_\odot\ \text{year}^{-1}$, followed by two quarter-periods with rates of 3×10^{-9} and $3 \times 10^{-7}\ M_\odot\ \text{year}^{-1}$. The lowest rate most closely corresponds with the expected behavior of Z Cam at minimum light, but the two higher rates were used to produce a more rapid density buildup than could otherwise be followed and to examine the effects of varying the rate. Results are displayed as a series of automatically generated contour plots of various physical quantities. In the plots, breaks in contours appear where lines cross zone boundaries, as a consequence of the variation in cell sizes. At intervals of 0.01P or 0.02P a complete set of plots was generated during the integrations; only a small, representative sample of those can be reproduced here. The integrations required nearly 11,000 time steps, generally of 3 s duration. Not described in the discussion of the numerical method, but in use during the calculation, is a density cutoff: cells with a column density less than $10^{-4}\ \text{g cm}^{-2}$ are set to zero density to avoid wasting effort on possibly spurious regions of the flow.

The outer boundary represents a flux of isothermal, 5000 K gas traveling radially inward at the sound speed, 12 km s^{-1} (with the atomic weight of one half). The angular column density distribution at L_1 is analogous to that employed to represent the z distribution:

$$\sigma(\theta) = \sigma(L_1) \exp\{-[\psi(\theta) - \psi(L_1)]/T^*\}. \quad (32)$$

This implies an assumption that the red star corotates with the binary, as seems reasonable in such short-period systems. Near L_1 the Roche potential increases

steeply with angle, relative to the thermal energy of the gas. Consequently, the stream is quite narrow; the density is reduced by a factor of 10^4 only 4° from L_1. The density distribution is scaled to produce the appropriate mass transfer rate. At $3 \times 10^{-9}\ M_\odot\ \mathrm{year}^{-1}$ the column density, 30 g cm^{-2}, and the scale height 1.5×10^9 cm, produce a mean density near L_1 of 2×10^{-8} g cm^{-3}, which is not unreasonable for the outer atmosphere of a dwarf G star.

Since the flow near L_1 comes into equilibrium slowly, an initial calculation was performed which considered only the grid with $r/a \geq 0.2$, and started with an empty grid. After 0.4P that region was completely in equilibrium. The results are displayed in Figures 1 and 2. The position and velocity along the maximum density ridge closely match the corresponding particle trajectories. The broadening of the flow arises from pressure terms which create the initial spread at the boundary, and subsequent widening along the stream. These results serve as the starting point, time 0.0P, for the complete grid calculations which follow.

During the next 1.0P the flow quickly forms a ring which steadily increases in density, and a "hot spot" forms. The results are illustrated by graphs of the flow after 0.07P, 0.29P, and 1.0P.

After 0.07P the flow is broadly dispersed through the Roche lobe following passage of the gas around the white dwarf. Figures 3, 4, and 5 present the density, temperature, and velocity at this time. The central grid remains empty because the gas has too much angular momentum to penetrate close to the origin. The stream from L_1 to the white dwarf creates an important obstacle to the dispersed, lower-density, returning gas. A shock forms along the interface between the two parts of the flow, and a large amount of energy is liberated as radiation by the heated gas. As this less energetic gas continues to circuit the star, it is drawn into tighter orbit. A high temperature is apparent in the long shock only where the density is great enough to prevent virtually instantaneous cooling.

By 0.29P a thick, dense ring has formed, as is apparent in Figures 6, 7, and 8. The ring density, as high as 50 g cm^{-2}, is great enough to dominate the stream, in the sense that the stream is no longer able to force itself through the central regions sending gas into the outer Roche lobe. The gaseous interaction is now concentrated at the intersection of ring and stream, where a hot spot, with a maximum temperature of 2×10^4 K, is evident.

No dramatic changes occur in the flow during the next 0.8P; the basic transformation to a stream and ring structure is complete. However, interesting variable features occur. The location of maximum temperature in the spot wanders in angle between about 225° and 270°. Also, the outer edge of the disk frequently "spins off" gas at low density into the outer Roche lobe. Individually these features are short-lived since they are destroyed after being swept back into the higher density stream from L_1. Several of these low-density protrusions are visible in the detailed plots, Figures 7–11, representing the gas after one period of mass transfer at a constant rate of $3 \times 10^{-8}\ M_\odot\ \mathrm{year}^{-1}$. Note that away from the spot most of the gas has cooled to low temperatures. Contours inside about 0.09 in r/a are confused by a large radial density variation. The low-density central regions are cut off from the outside regions by the higher density ring.

After an additional quarter-period of reduced mass transfer at a rate close to that expected in Z Cam, the grid is plotted in Figures 12–18. Two differences are immediately apparent. First, there is a well developed low-density stream leaving the grid, but the stream has not actually acquired sufficient velocity to escape the Roche lobe. This stream is probably only a transient; it formed at 1.18P. Several similar, but less well developed, streams appear and die away during adjustment to the lower mass transfer rate. These streams penetrate much farther into the Roche lobe than those protrusions formed at the constant transfer rate. Second, the hot spot, though interestingly maintaining nearly the same maximum temperature, definitely decreases in size. Aside from these changes, no alterations in the basic flow are apparent, which is to be expected since the stream is now merely a perturbation acting on the ring.

To examine the effects of rapidly enhanced mass transfer, a final quarter-period of gas flow was calculated at $3 \times 10^{-7}\ M_\odot\ \mathrm{year}^{-1}$; such a high rate might occur during outbursts if accretion heating produces the luminosity increase. The results at 1.50P are plotted in Figures 19–21. While the disk still dominates the stream, much greater penetration of the disk occurs before the stream is stopped. Consequently the spot broadens and rotates farther around the white dwarf. The spot's maximum temperature reaches 60,000 K. Low-density protrusions again form along the disk's outer edge. Finally, note that the disk's outer radius is increased since the stream feeds an appreciable amount of gas along the outer disk, and the spot further deflects the flow outward.

In integrated luminosity during the first 1.0P the grid rapidly reaches a state liberating $(5.6 \pm 0.2) \times 10^{33}$ ergs s^{-1}. The variation about the mean is irregular, but insufficient to represent the observed flickering. With the mass transfer rate reduced by a factor of 10, the luminosity decreases by a factor of 7 to about $(8 \pm 1) \times 10^{32}$ ergs s^{-1}. Further decrease might occur since the variability is too large at 1.25P to be certain that equilibrium is established. At the highest mass transfer rate the final luminosity is $(5.2 \pm 0.6) \times 10^{34}$ ergs s^{-1}, but, again, the luminosity is still quite variable at 1.50P. Note that the integrated grid luminosity is nearly synonymous with spot luminosity. As a detail, when the transfer rate is altered, not only is the boundary influx of mass changed, but, simultaneously, all column densities outside r/a of 0.4 are appropriately rescaled. This process produced a density discontinuity in the stream from L_1 which is blurred numerically as it propagates toward the ring. Nonetheless, the luminosity rapidly adjusts to the variable mass transfer rate. In decreasing the rate at 1.0P, 80 percent of the luminosity decrease

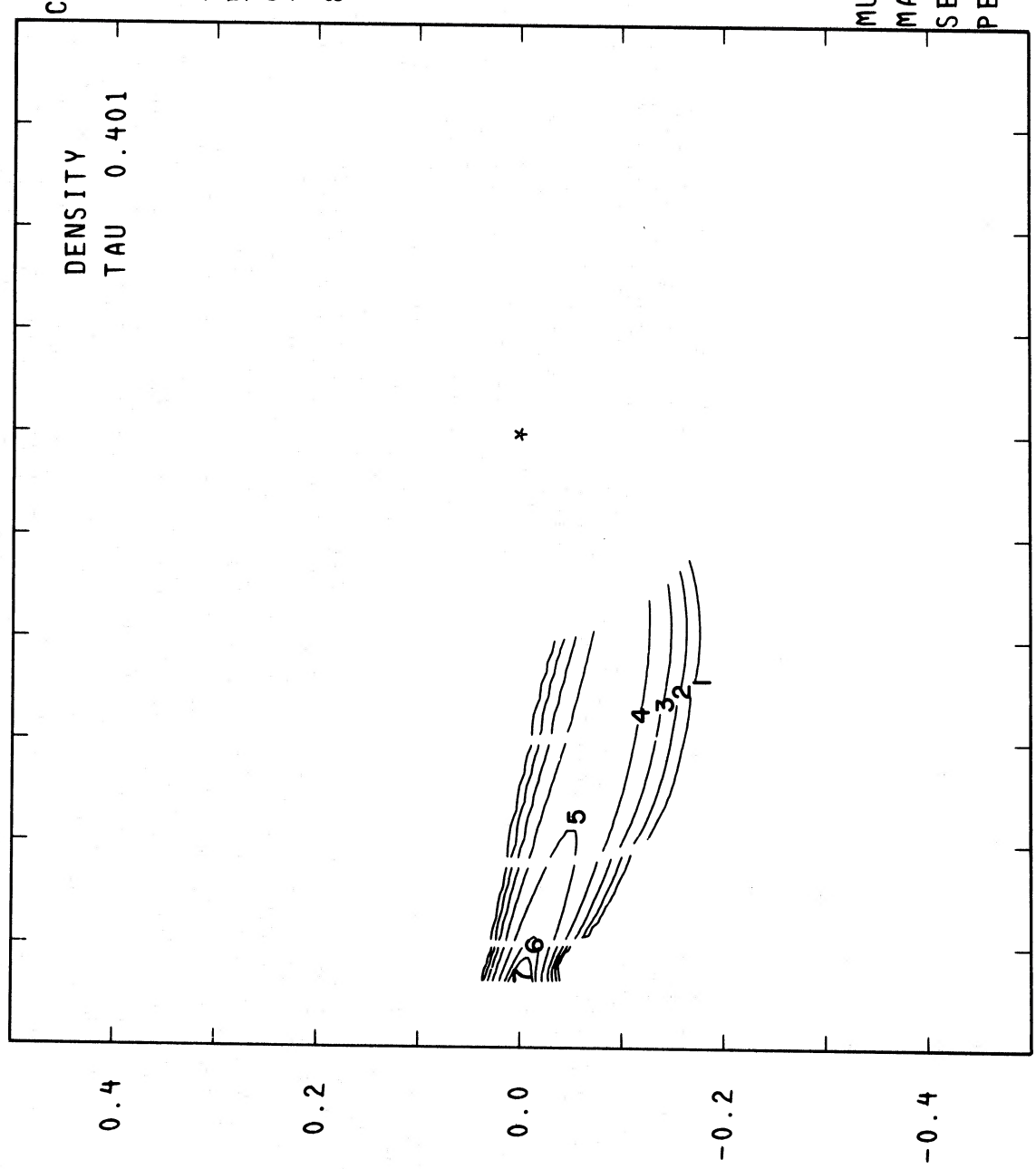

FIG. 1.—Column densities 0.4 orbital periods after injecting gas through L_1 into an empty grid. The mass transfer rate is $3 \times 10^{-8}\ M_\odot\ \text{year}^{-1}$, and the flow is not followed inside $r/a = 0.20$.

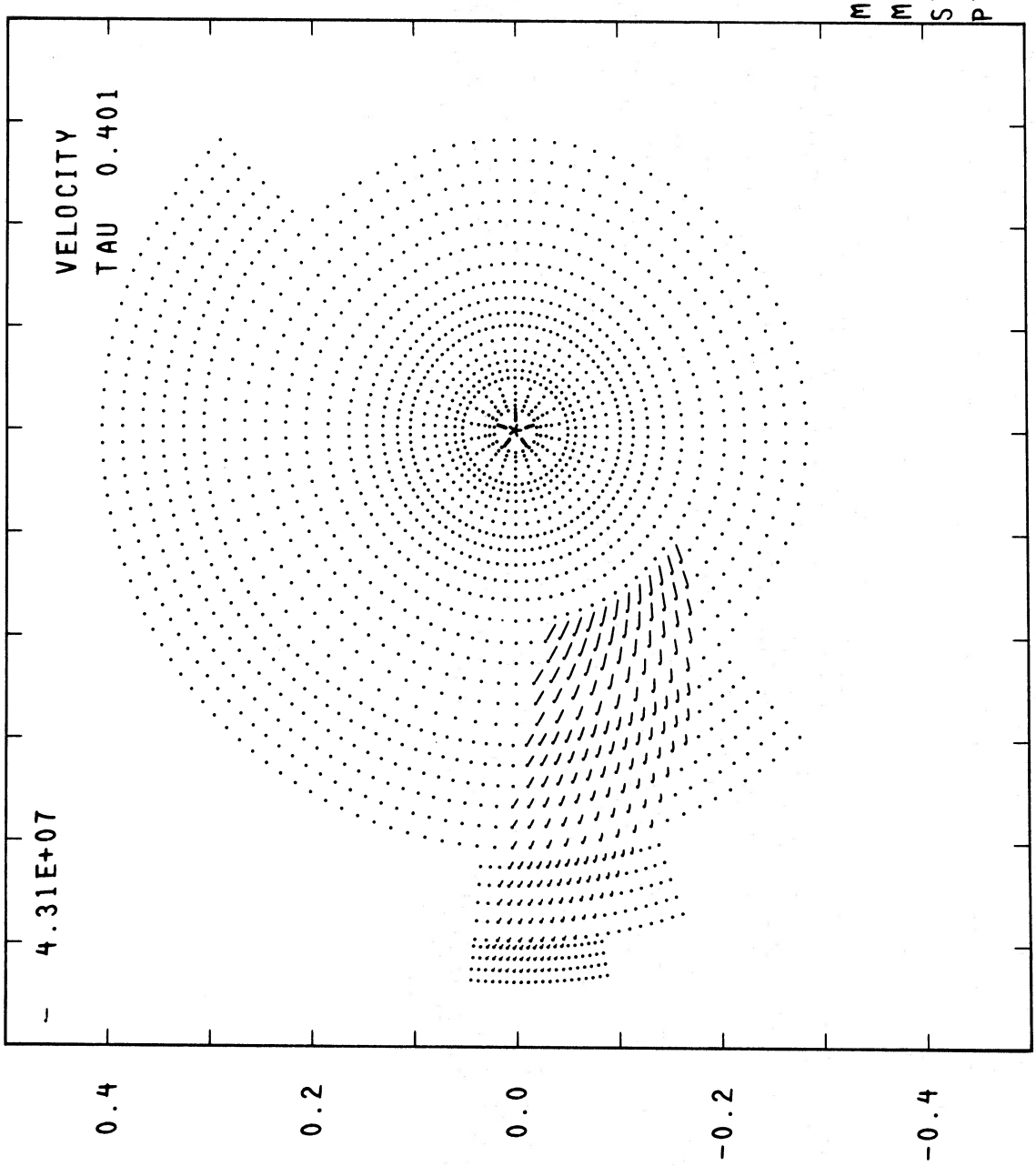

FIG. 2.—Velocity vectors for conditions as in Fig. 1. The dimensionless unit velocity, 431 km s^{-1}, is indicated in the upper left-hand corner. Dots represent the centers of cells, but only every other cell in r and θ is shown. No vector is drawn if a cell is empty.

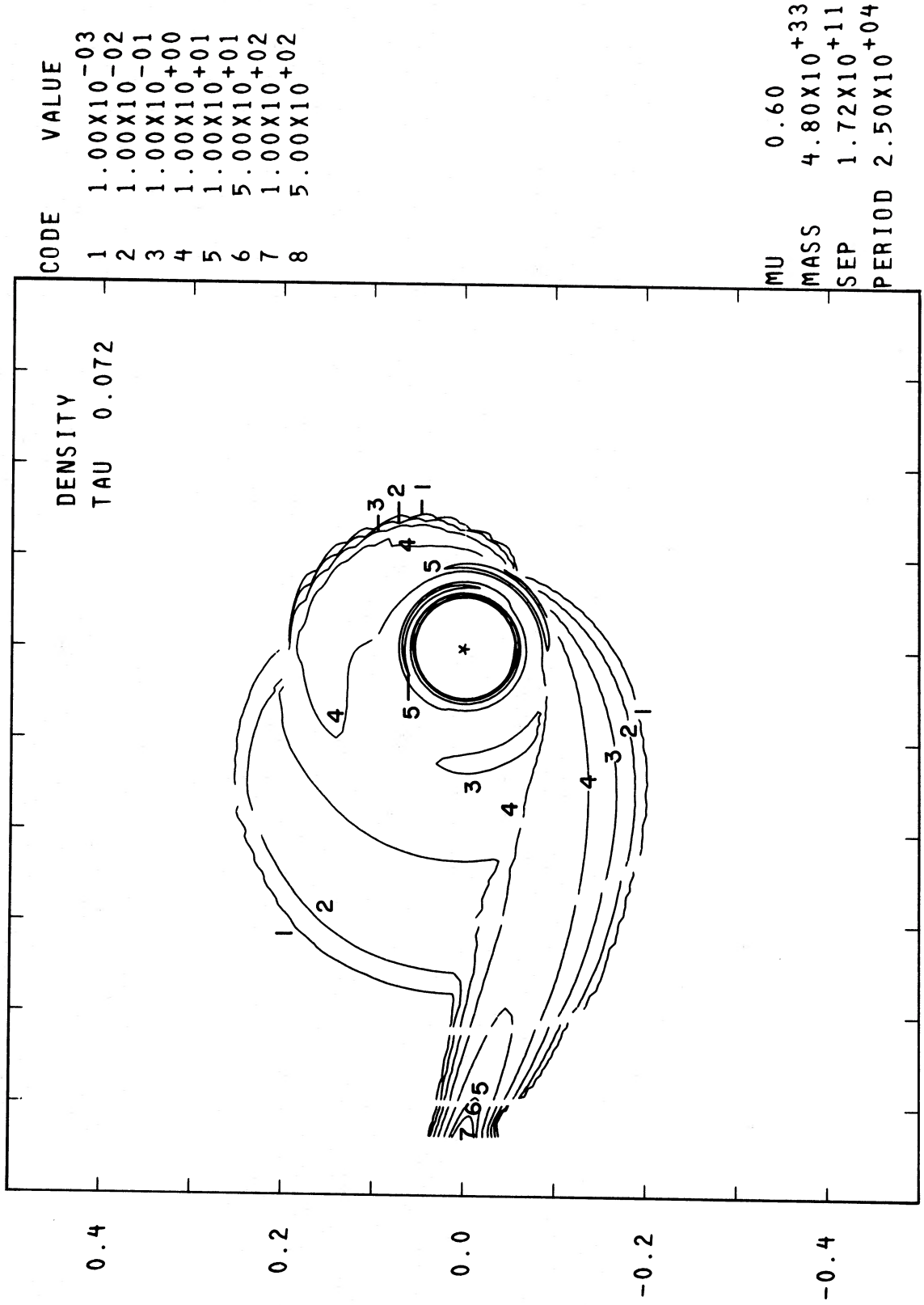

FIG. 3.—Column density contours 0.07P after continuing the flow from conditions as in Fig. 1

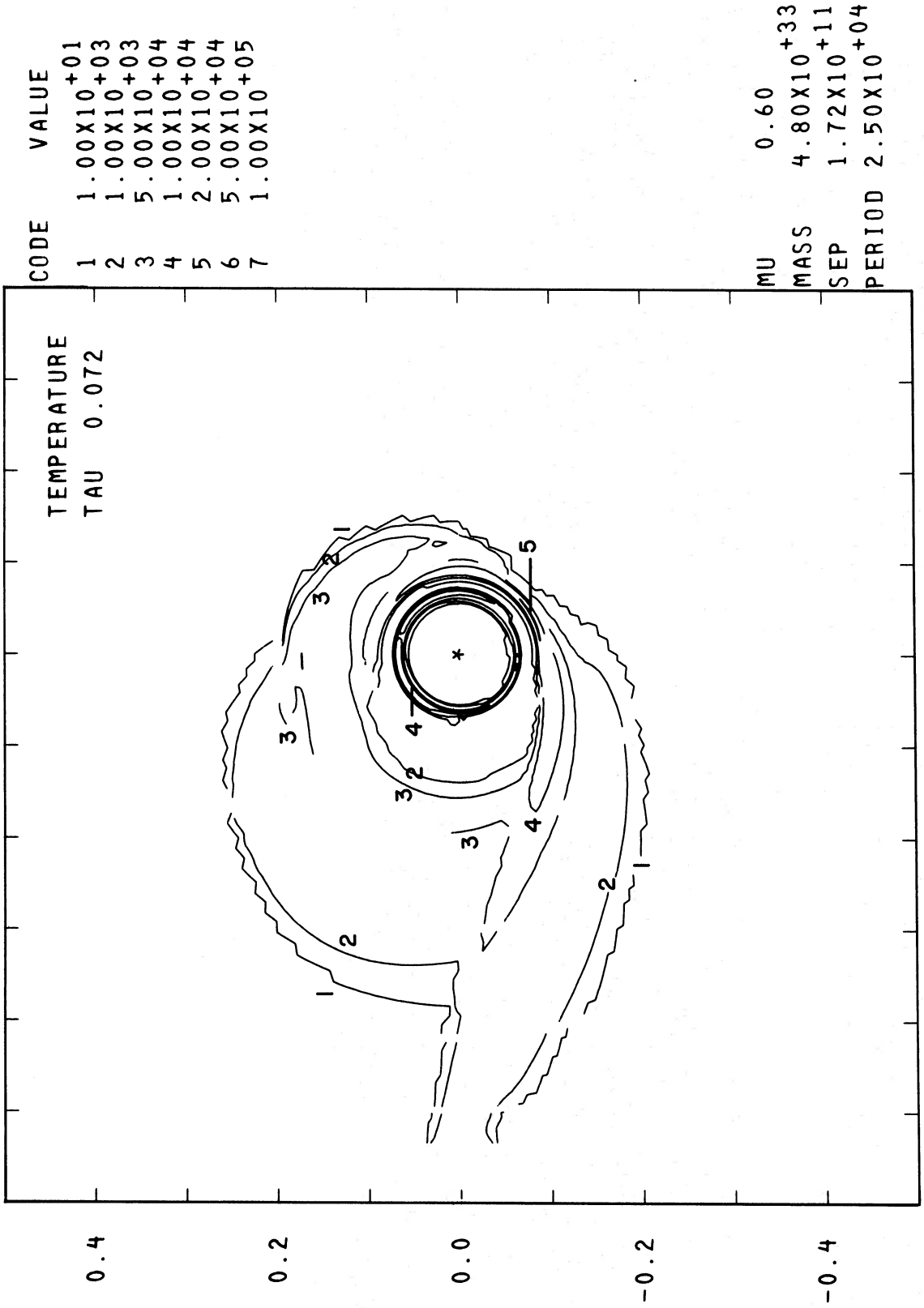

FIG. 4.—Temperature at 0.07P. Note the long, broad shock front; the cause of the shock is apparent from the next figure.

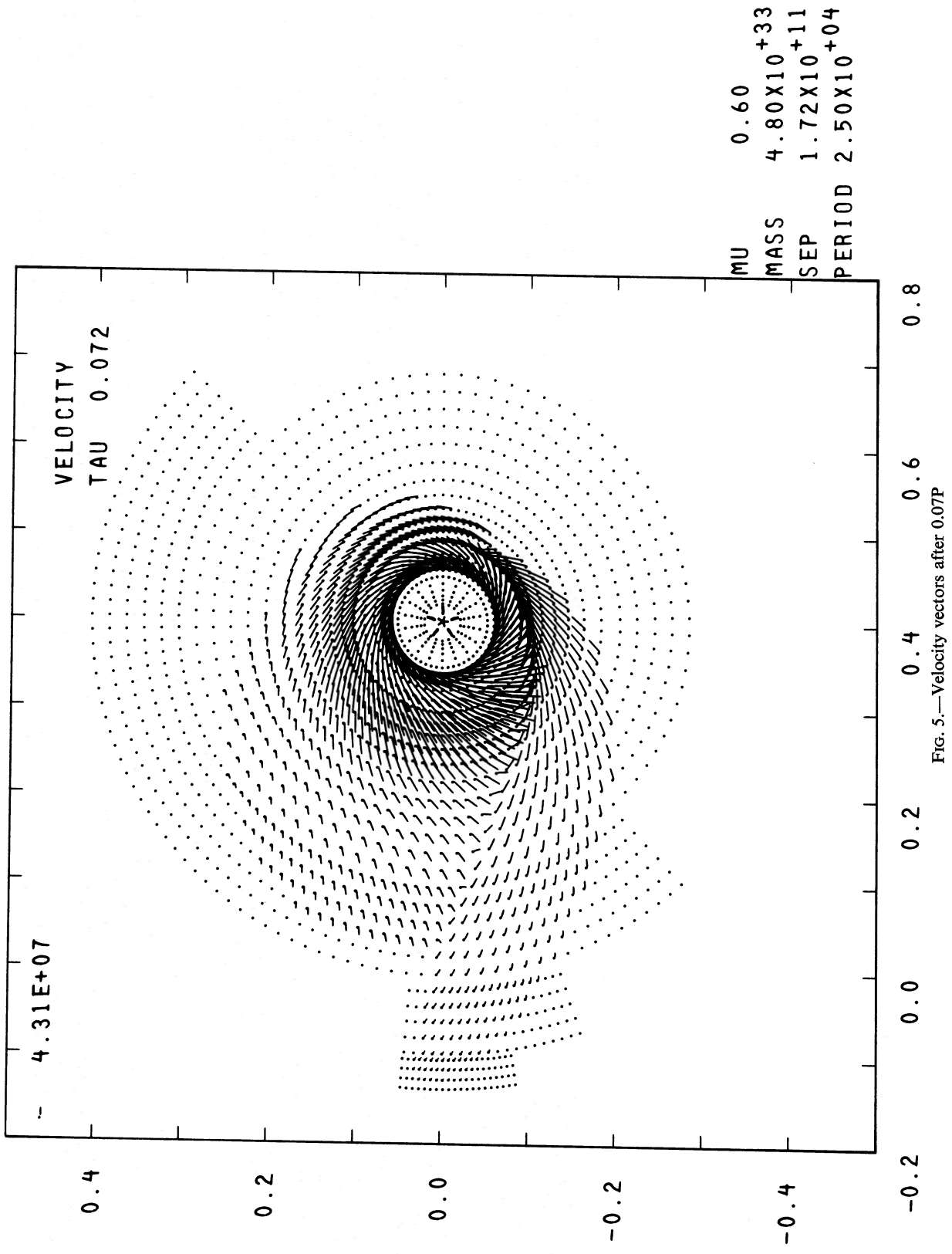

FIG. 5.—Velocity vectors after 0.07P

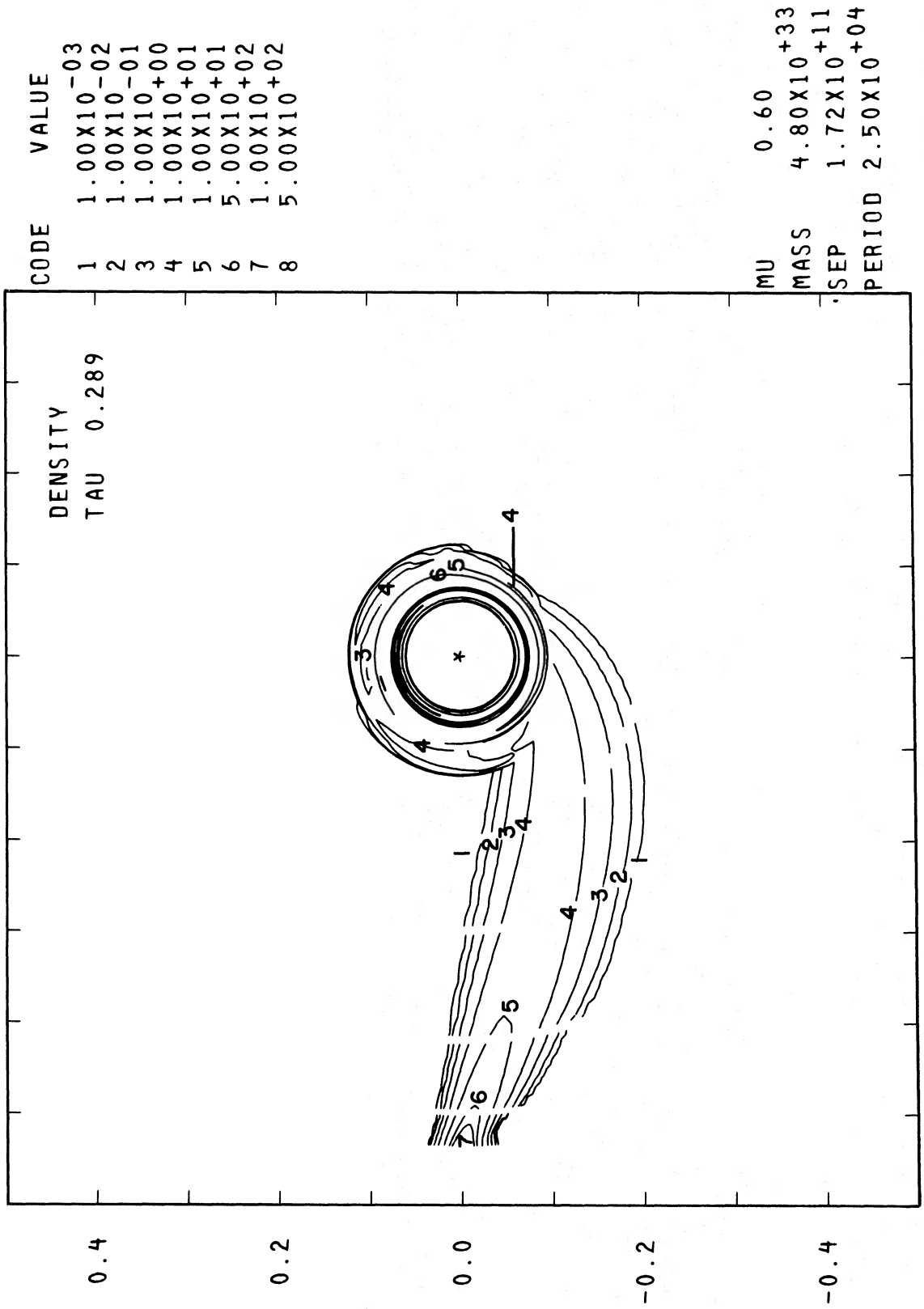

FIG. 6.—Column density contours after 0.289P. The disk stream structure is evident.

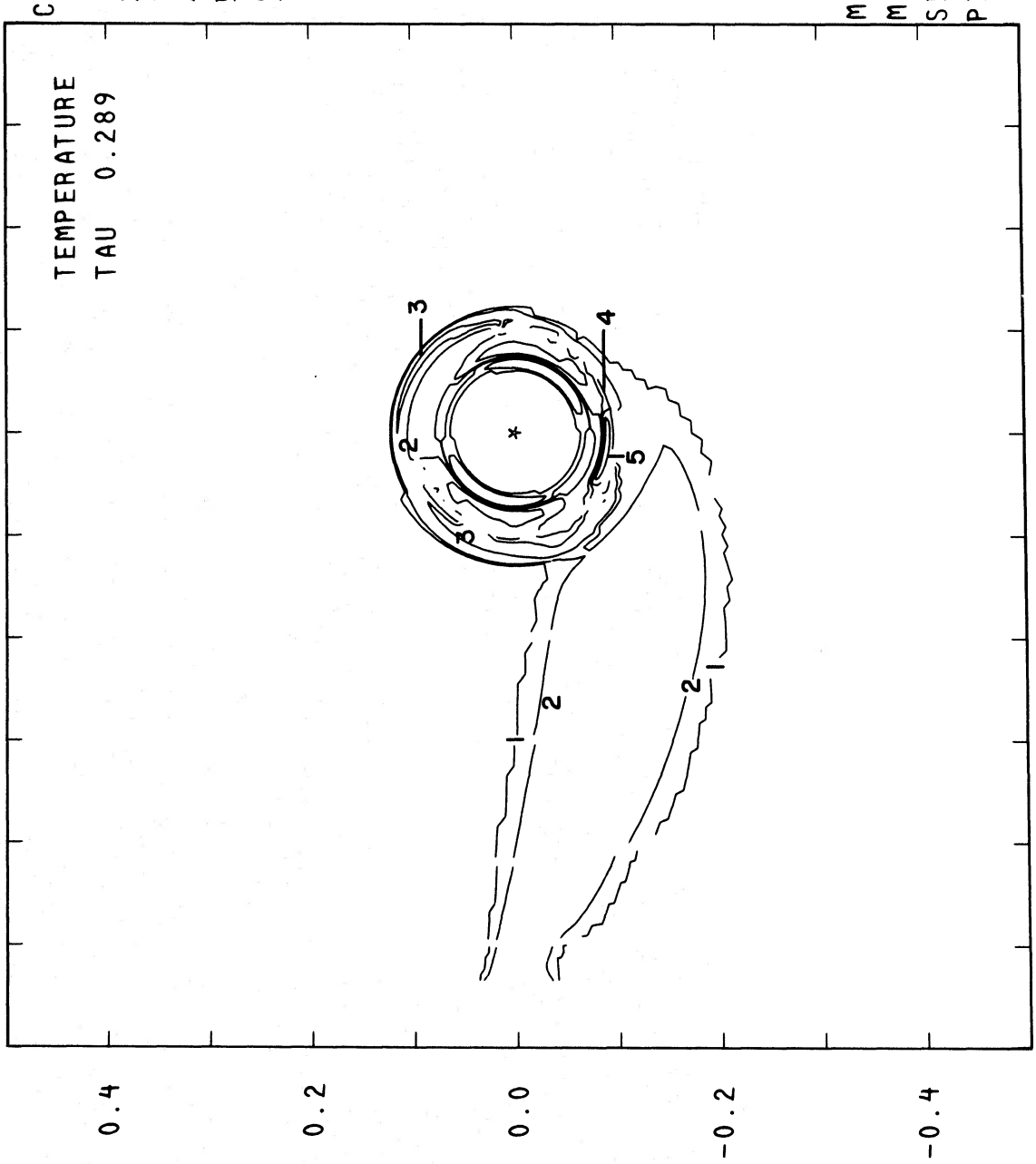

FIG. 7.—Temperature after 0.289P. A hot spot with temperatures reaching 20,000 K is present at the intersection of disk and stream, but most of the other gas is at low temperatures.

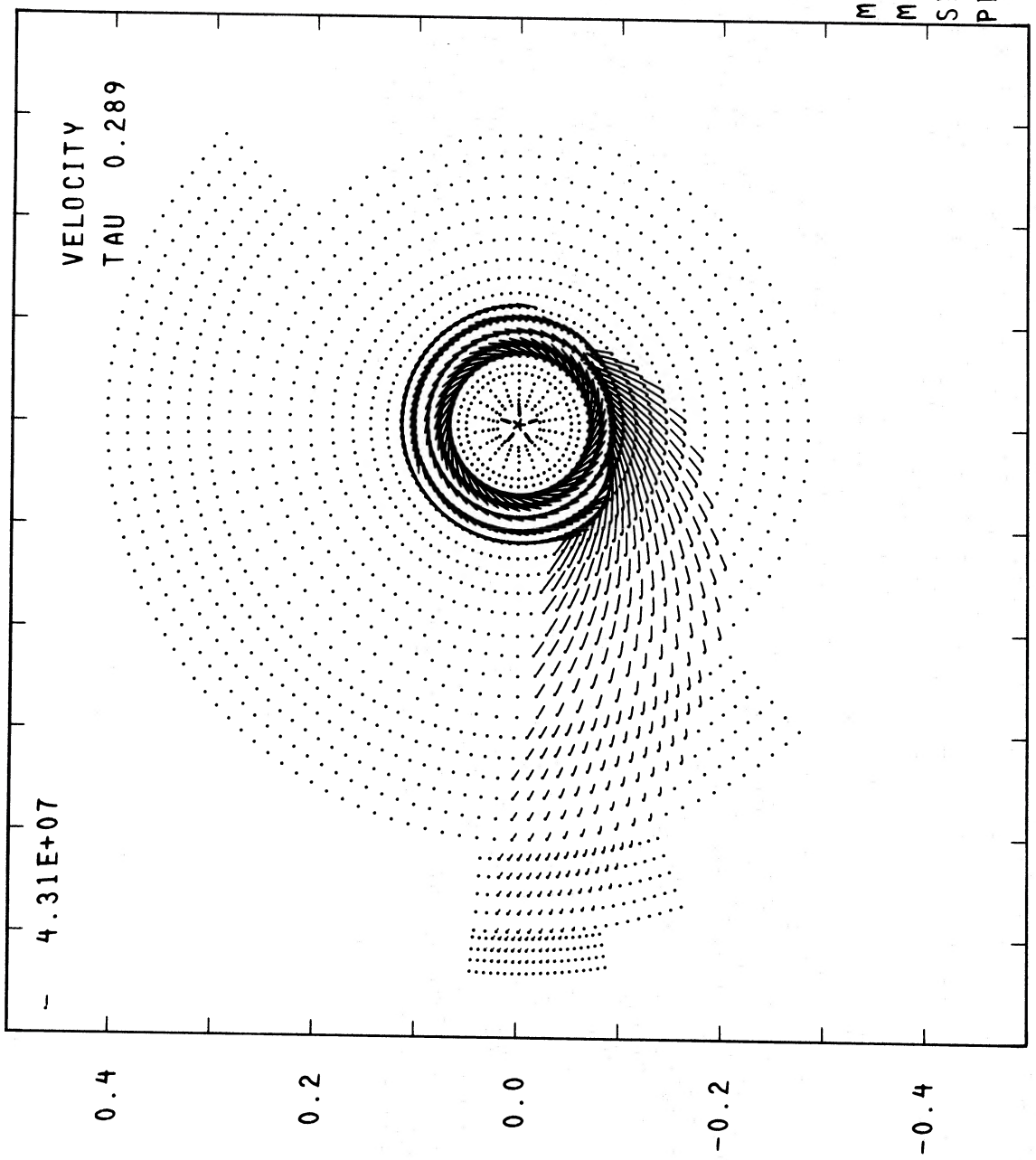

FIG. 8.—Velocity vectors after 0.289P

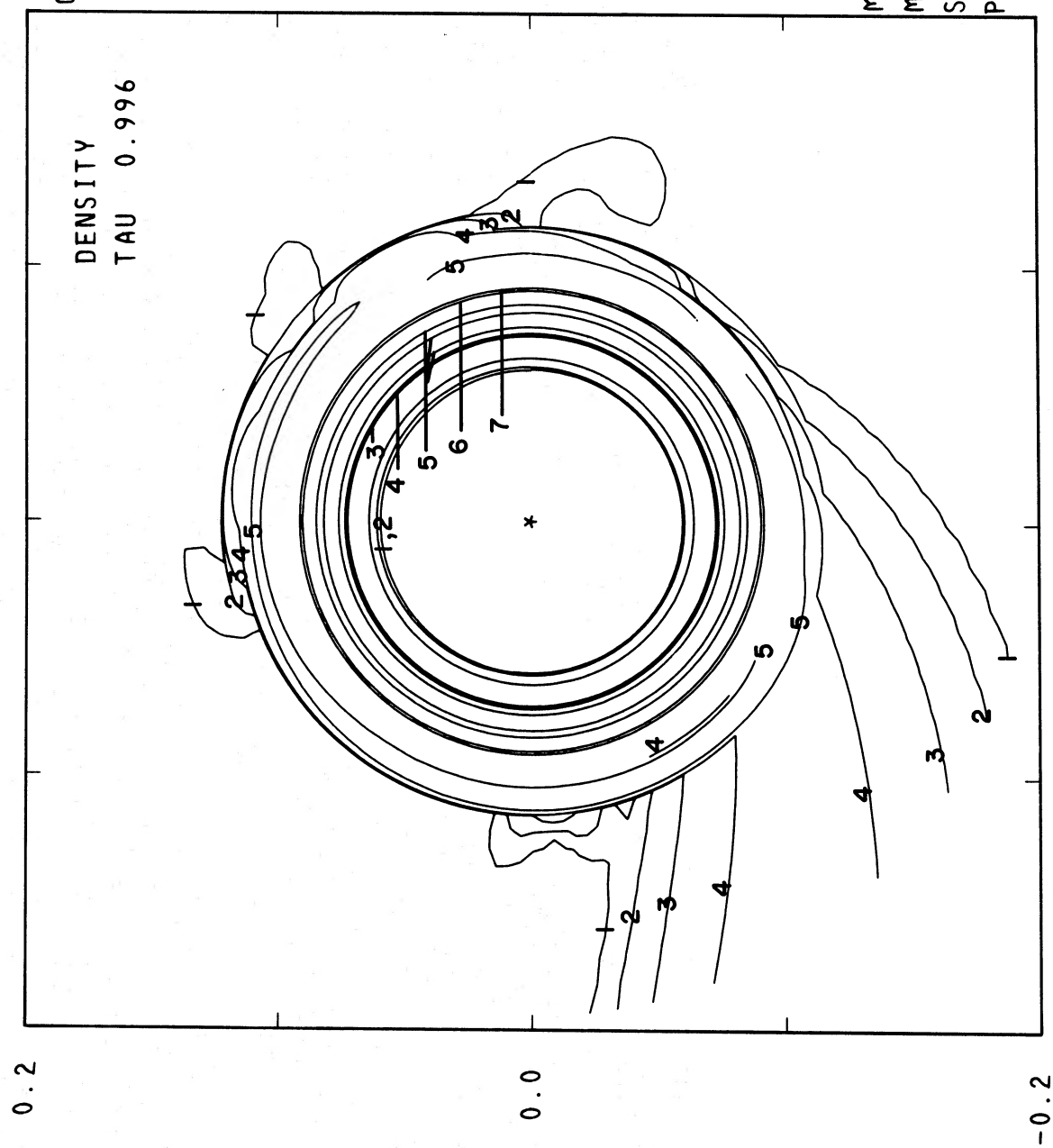

FIG. 9.—Column density contours after 1.0P of mass transfer at $3 \times 10^{-8}\ M_{\odot}\ \text{year}^{-1}$. Note the low-density protrusions along the outer edge of the ring.

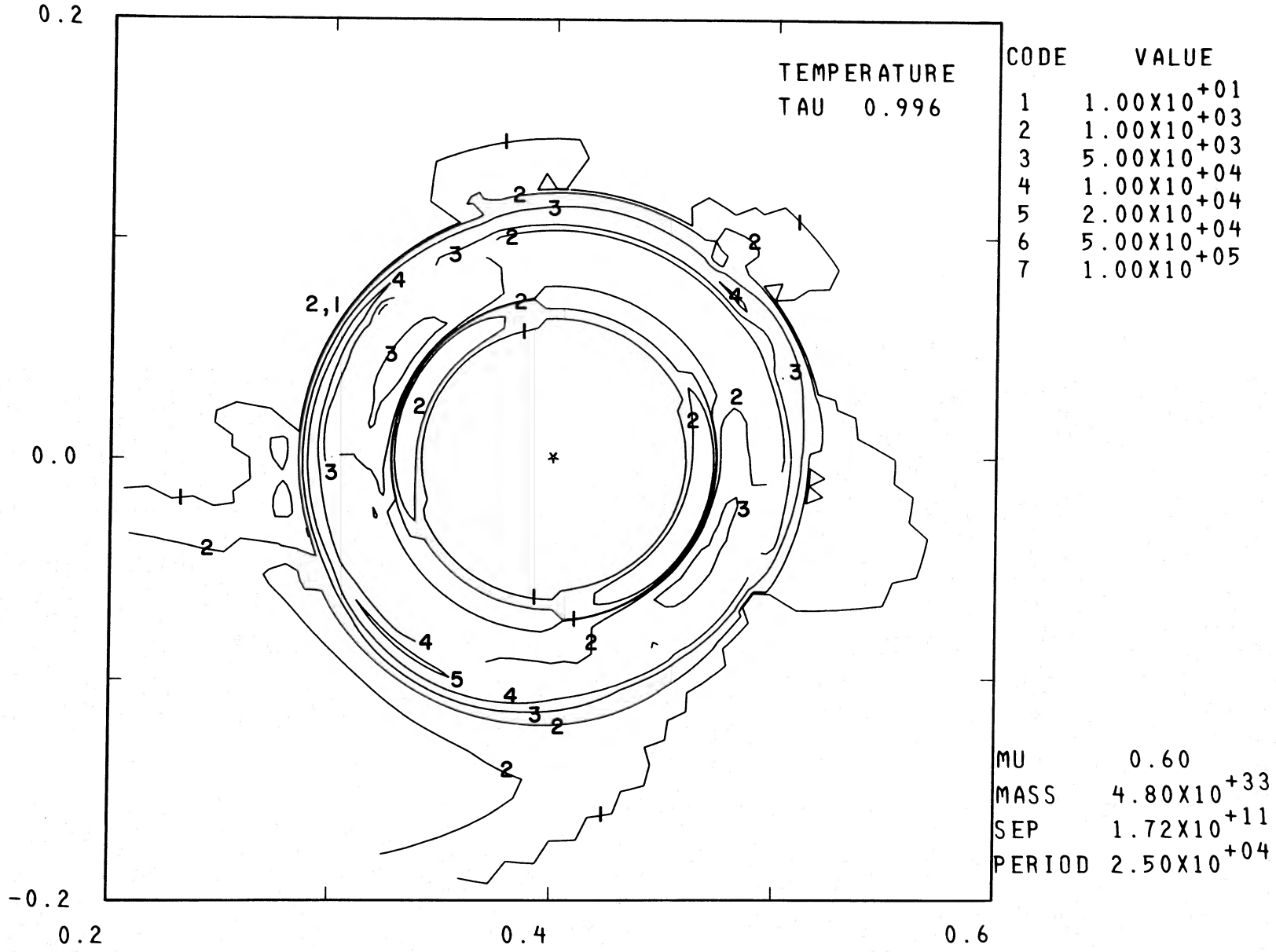

FIG. 10.—Temperature after 1.0P

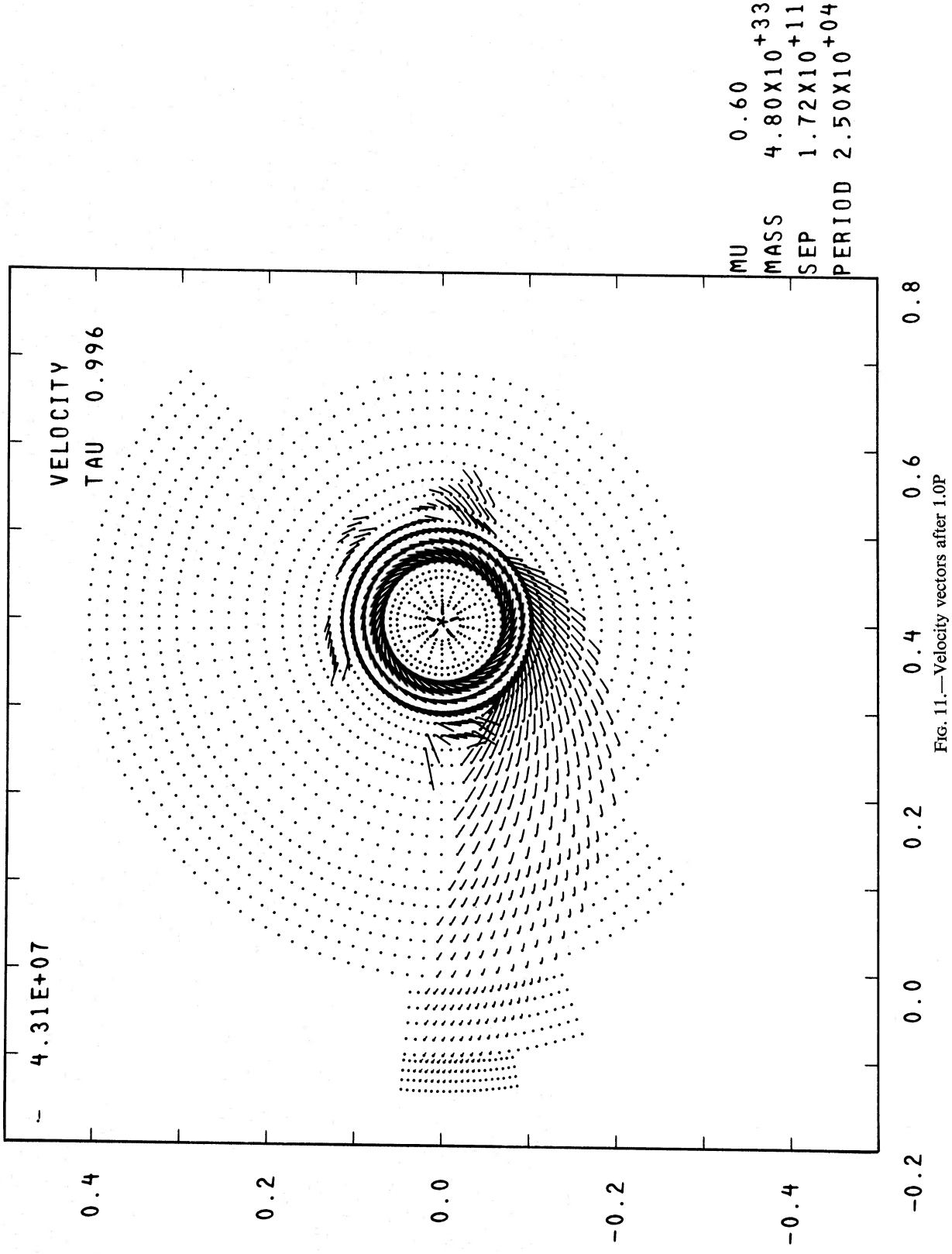

FIG. 11.—Velocity vectors after 1.0P

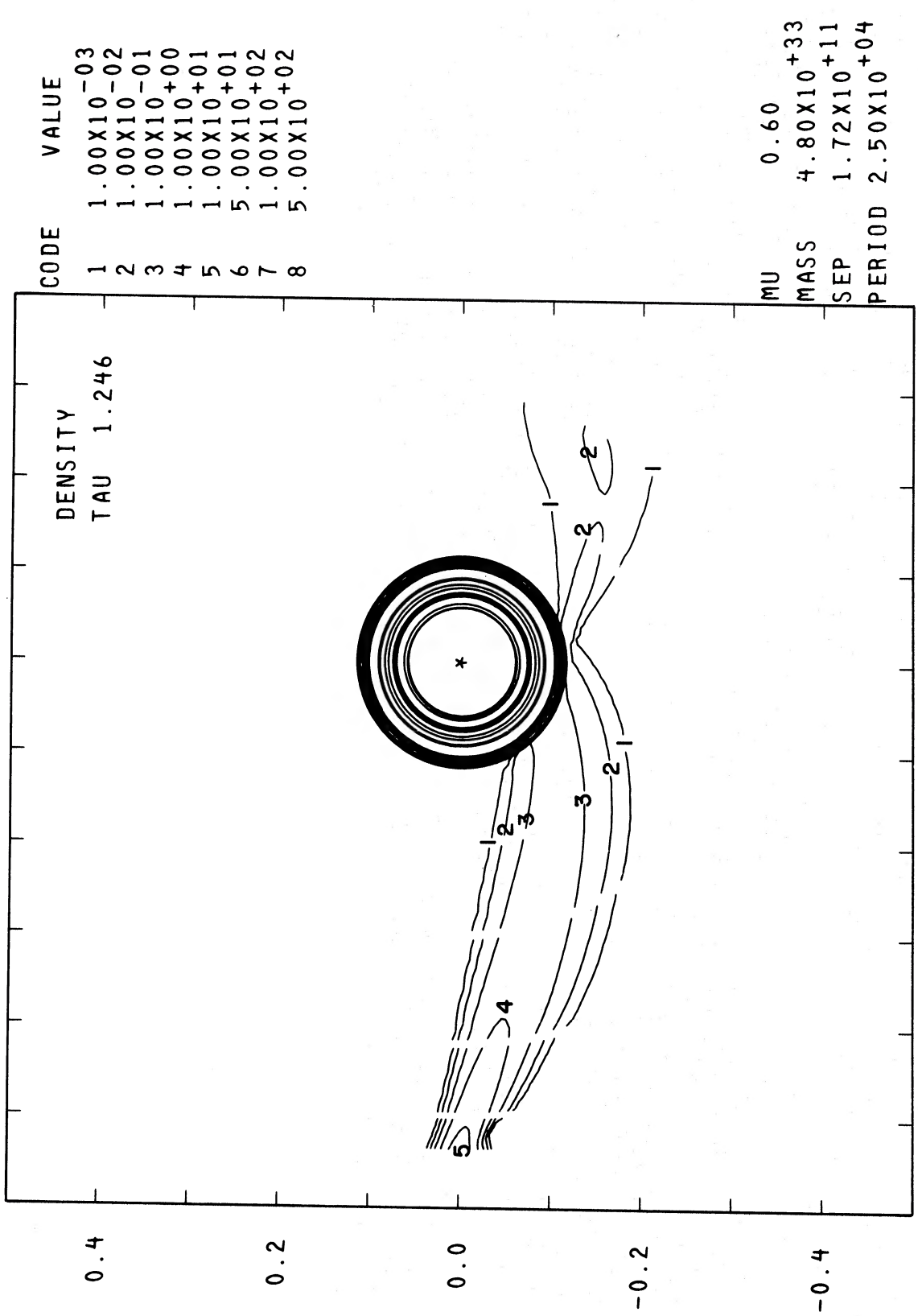

FIG. 12.—Column density contours after 1.25P. The transfer rate was reduced by a factor of ten at 1.0P. The low-density stream leaving the grid is probably only a transient. It actually has insufficient energy to escape the white dwarf's Roche lobe.

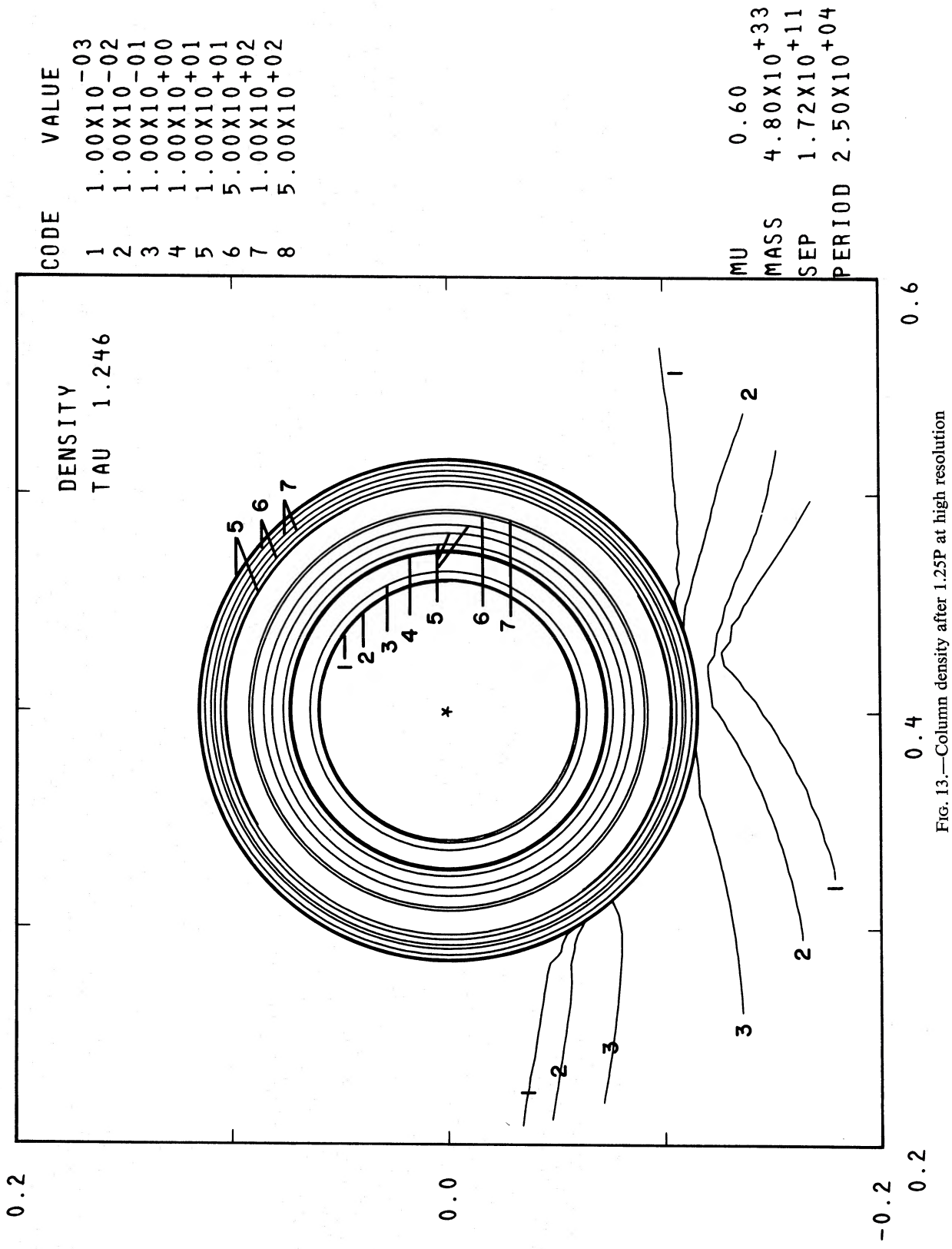

FIG. 13.—Column density after 1.25P at high resolution

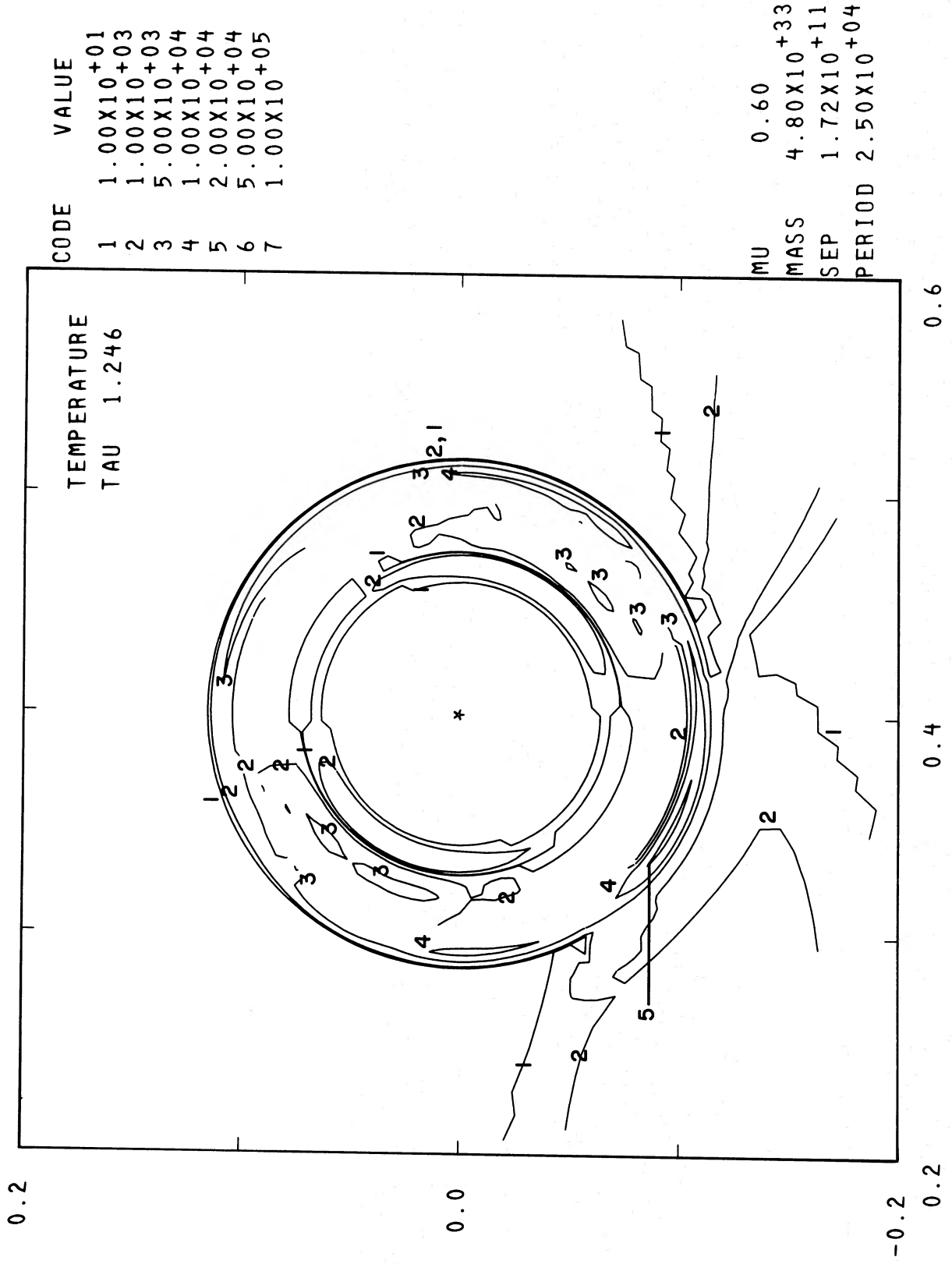

FIG. 14.—Temperature after 1.25P

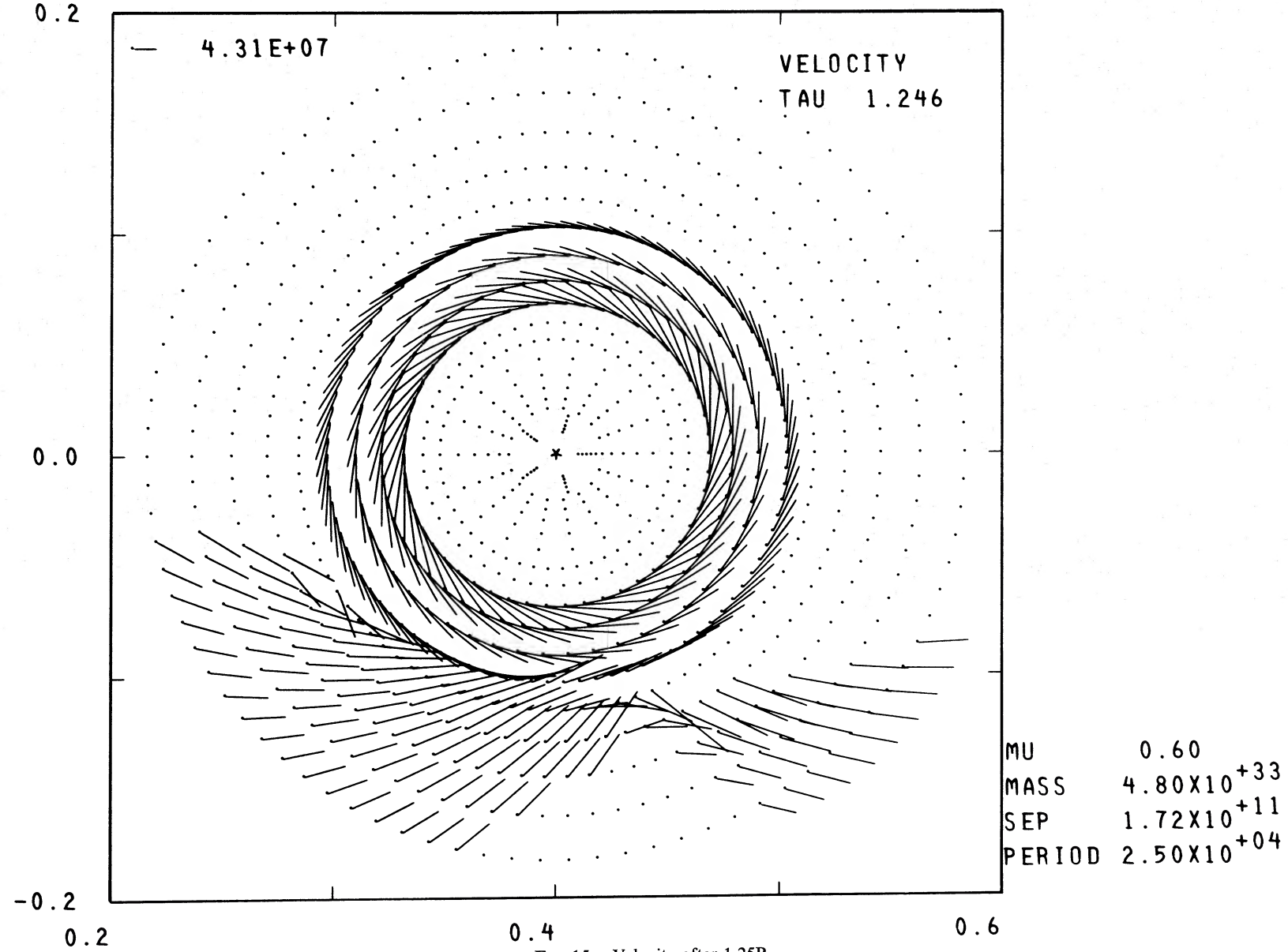

FIG. 15.—Velocity after 1.25P

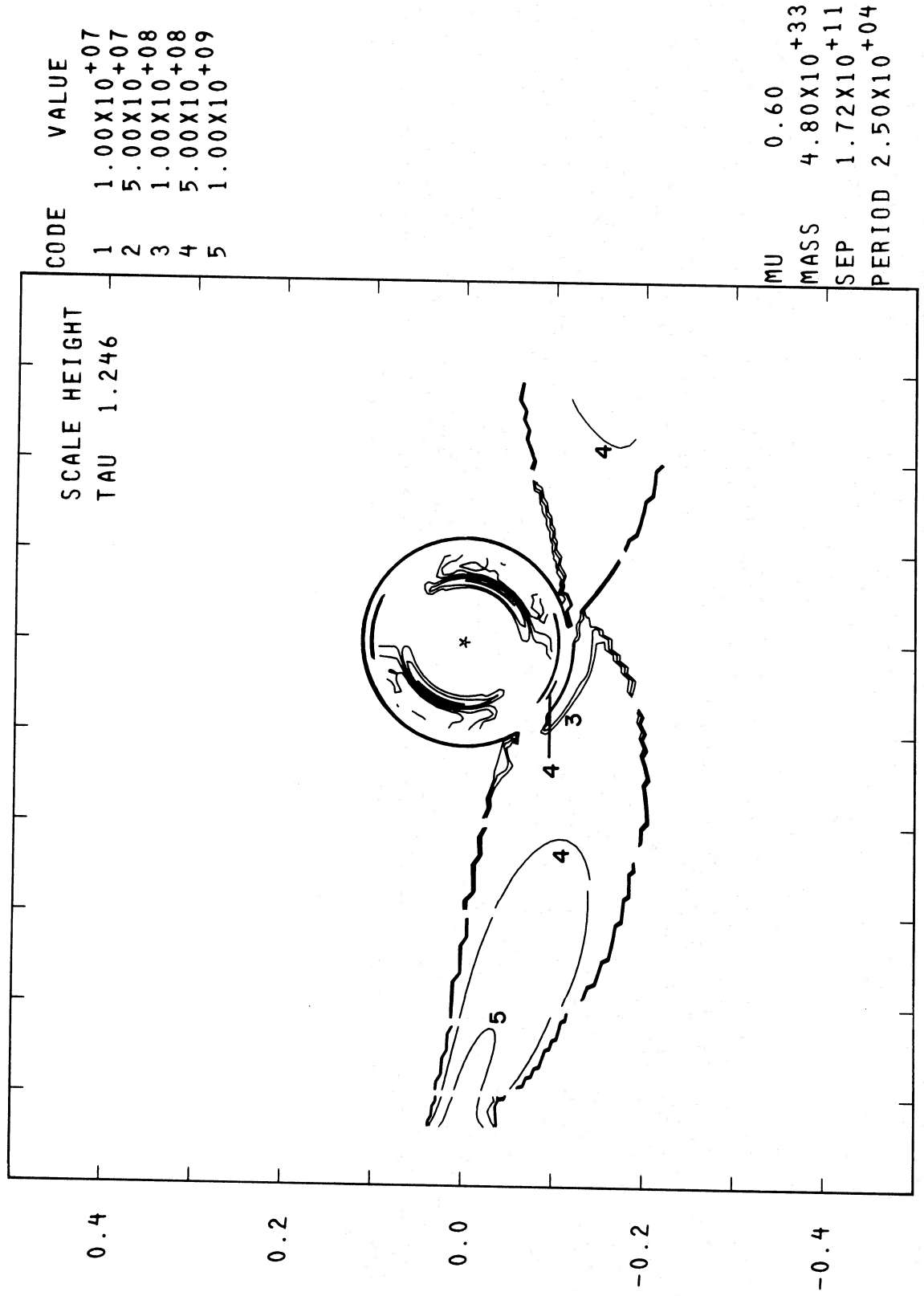

FIG. 16.—Scale-height contours after 1.25P

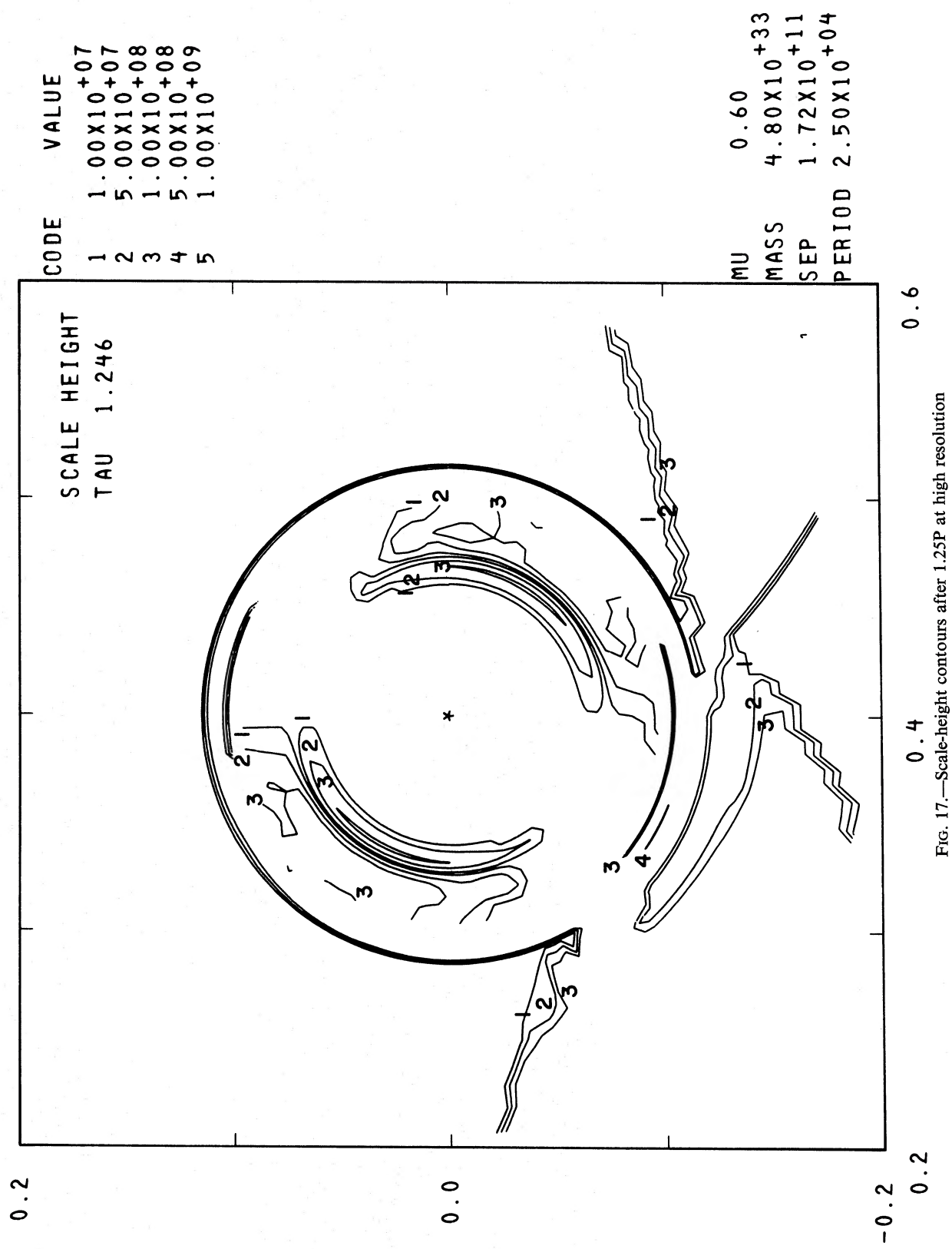

FIG. 17.—Scale-height contours after 1.25P at high resolution

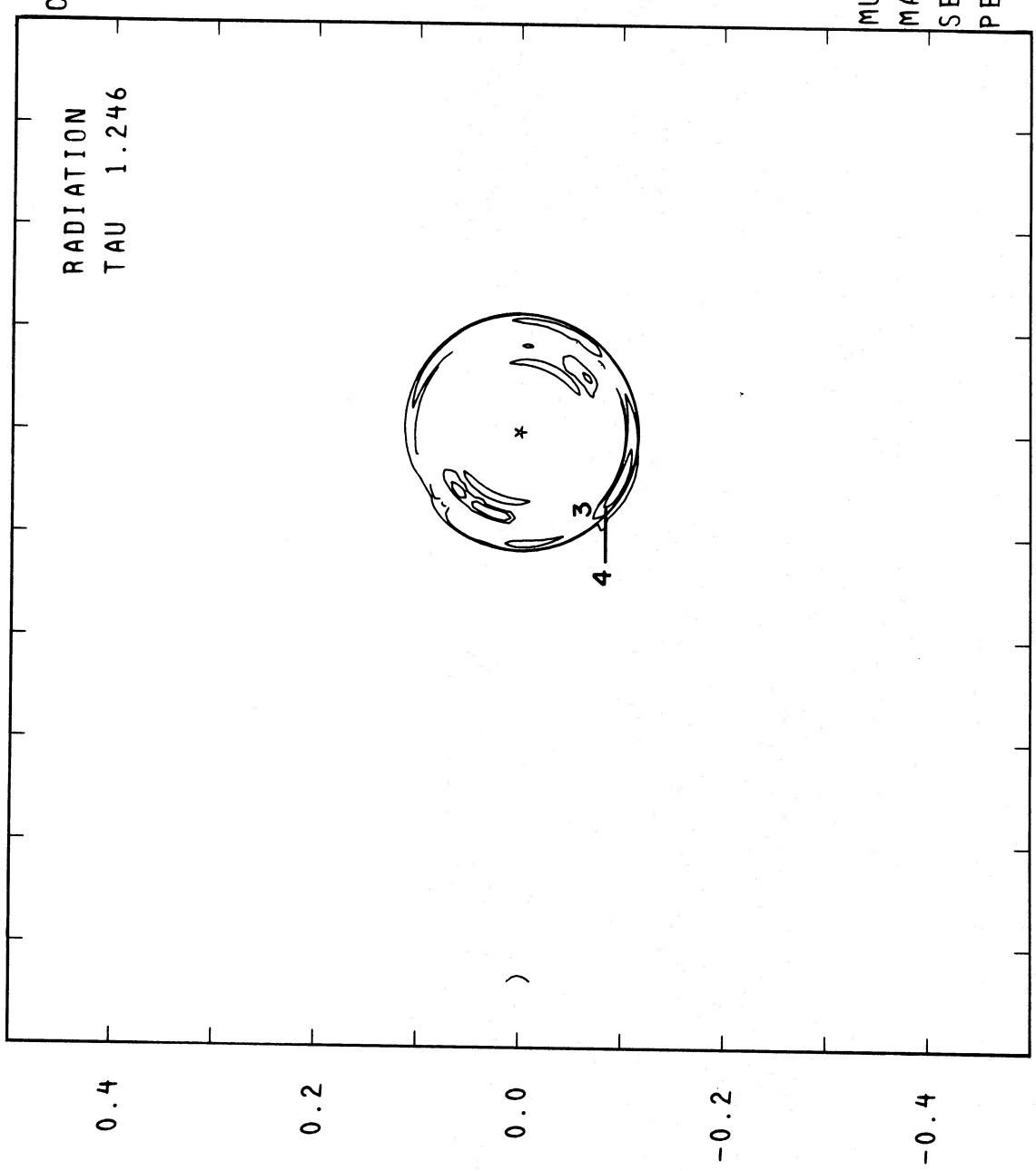

FIG. 18.—Radiative emission per unit surface area after 1.25P (in units of 10^{12} ergs cm^{-2} s^{-1})

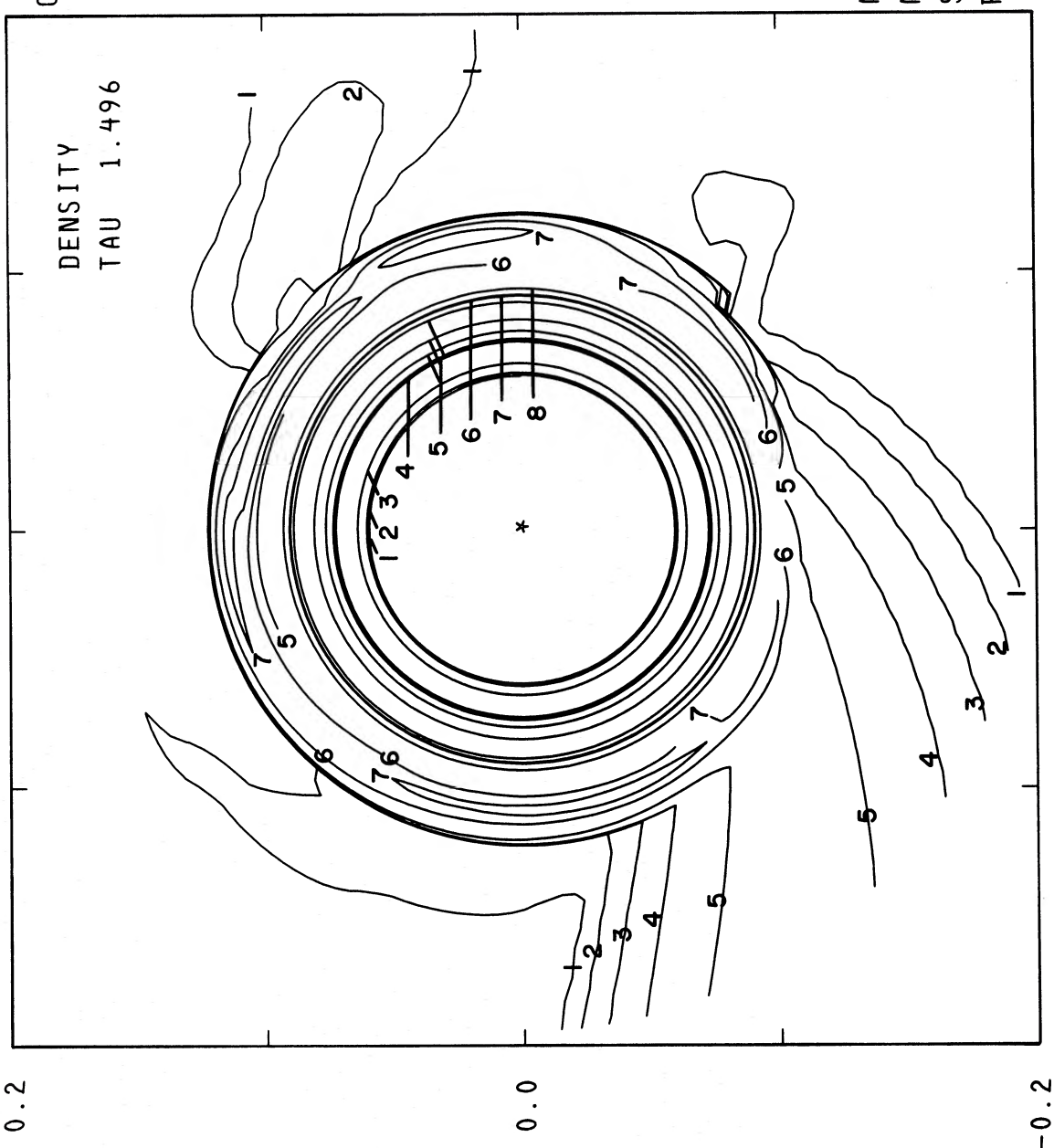

FIG. 19.—Column density after 1.50P. The transfer rate increased to $3 \times 10^{-7}\ M_{\odot}\ \text{year}^{-1}$ at 1.25P.

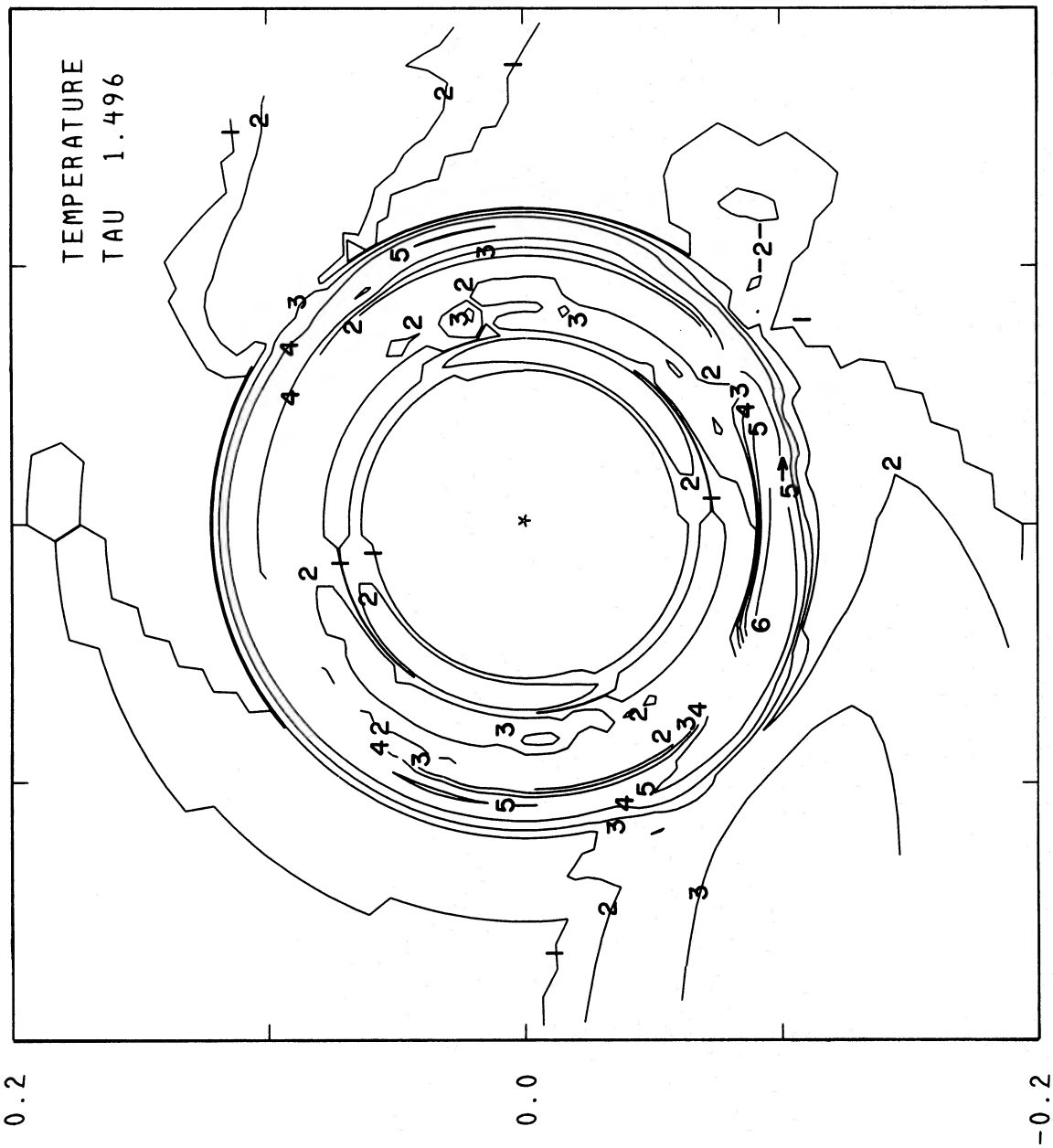

FIG. 20.—Temperature after 1.50P

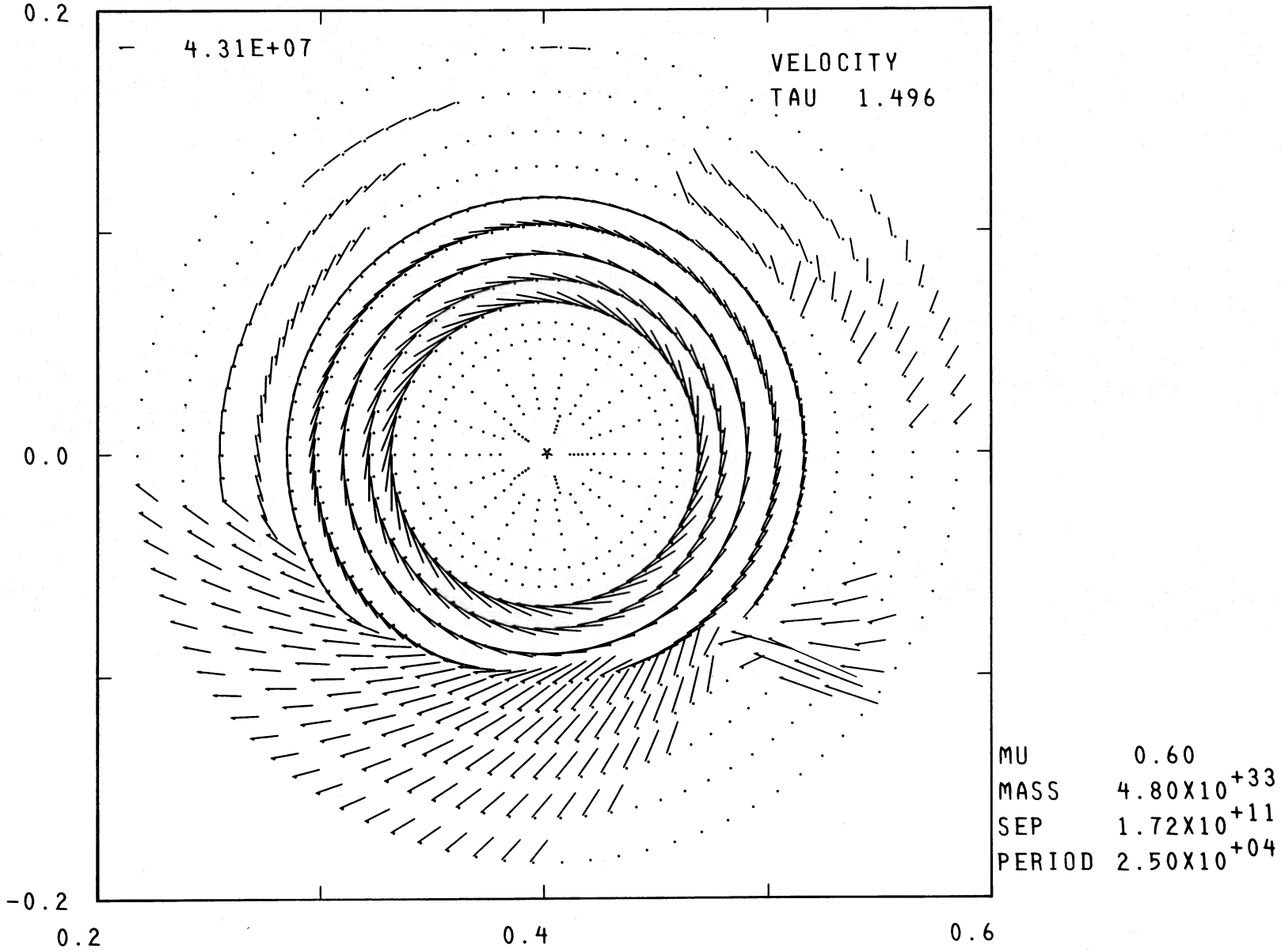

FIG. 21.—Velocity after 1.50P

occurs in 0.01P, i.e., 4 minutes, while the increase in luminosity from 8×10^{32} ergs s^{-1} to 6×10^{34} ergs s^{-1} at about 1.25P requires only 0.03P.

A detailed numerical listing of the grid was made at 1.0P and 1.25P to examine the spot characteristics in detail. After one period the spot's maximum temperature, 22,000 K, is situated in the cell centered at $r/a = 0.109$, $\theta = 230°$. Temperatures in excess of 15,000 K extend in an angle from 210° to 258°, while the spot also extends into a few cells centered at $r/a = 0.103$. The spot's column density of 30 g cm^{-2} implies that the hot spot is optically thick. At the reduced flow rate the spot moves to $\theta = 242°$, extending from 228° to 264° for temperatures greater than 15,000 K, and is entirely confined to cells centered at $r/a = 0.109$. The maximum temperature increase slightly to 23,000 K, and the column density is now 114 g cm^{-2}. The higher density seems to be a result of a complete readjustment of the ring such that the high-density region has been able to move outward, since the stream exerts less pressure against the ring at the spot. The spot angles are only instantaneous values since wandering in phase persists throughout the 1.25 periods covered by the integrations. At the highest mass transfer rate the spot is broadened appreciably and reaches a maximum temperature of 64,000 K at $r/a = 0.096$, $\theta = 268°$. The column density is 10^3 g cm^{-2}.

Overall, throughout the flow the gas remains tightly confined to the plane in accordance with the assumptions. The largest scale height in the interior flow occurs at the hot spot, where the height of 5×10^8 cm is only 0.003 of the binary separation.

It should be pointed out that inside the dense outer ring gaseous motions are not well represented by the numerical method once the gas nears circular motion. While the force is still well represented, any remaining radial motions are dominated by the numerical mixing procedure. The overall density structure represents a slow relaxation to circular orbits. The gas is slowly moving outward to the radius appropriate to its angular momentum. In cross section the density displays two slopes upward to maxima. The first occurs at a zone boundary at $r/a \approx 0.109$. Eventually, all the gas would mix out to about 0.1 in r/a.

As the spot's size is primarily determined by the concentration of the stream, a final calculation was undertaken considering only the stream, but at much higher resolution to assess the affect of spreading caused artificially by the cell size. The density and velocity of the higher resolution stream are plotted in Figures 22 and 23. Although slightly narrowed, the stream is not significantly different from the lower resolution result.

The flow calculations presented have not achieved a steady state. While the mass transfer at $3 \times 10^{-8}\ M_\odot$ $year^{-1}$ did result in a nearly constant luminosity after 1.0P, the calculation at 3×10^{-9} and $3 \times 10^{-7}\ M_\odot$ $year^{-1}$ still showed strong variability after 0.25P. If the flow calculations could have been extended for longer periods, the spot would presumably establish itself at the same ultimate position in each case. However, the intervention of viscous evolution of the disk would certainly establish a different density distribution in the disk which would modify the hot spot's location. These results do show that the spot is rapidly established.

V. COMPARISON WITH PARTICLE TRAJECTORY MODELS

Particle trajectory calculations in the restricted three-body approximation provide a simple model for the position of the hot spot. The gas stream falling from L_1 obtains a particular angular momentum with respect to the blue star (in the nonrotating frame of reference) which is nearly conserved as the stream initially approaches and recedes from that star. If the stream's motion is approximated by a particle trajectory, both the stream's path and angular momentum can be found; and if the gas is assumed to acquire a Keplerian circular orbit about the blue star at a radius appropriate to its angular momentum, then the spot's position is determined by the intersection of the trajectory with the circular orbit. Such models were first calculated by Warner and Peters (1972), and later corrected by Flannery (1975). After a reduction to the standard dimensionless variables of the restricted three-body problem, the parameters describing the hot spot's location depend only on the relative masses of the stars comprising the binary (for low-velocity ejection at L_1).

For a mass fraction of 0.6, appropriate to the Z Cam calculations, the particle model provides the following parameters: the spot is located at $r/a = 0.103$, $\theta = 249°$, the circular velocity for gas in the ring is $V_c = 2.31$ (in the rotating frame of reference), and the energy difference between gas in the stream and ring at the spot is $\Delta E = 1.66$. (The velocity and energy difference are expressed in dimensionless units for which the scale factors are ωa and GM/a, respectively.) After 1.25P at the position of maximum temperature the hydrodynamic results show $r/a = 0.109$, $\theta = 242°$, $V_c = 2.24$, $\Delta E = 1.48$. Note that the grid's radial resolution places neighboring cells at $r/a = 0.103$ and 0.115, so the spot's position is partially governed by the limited resolution. An additional comparison is also possible. In the particle model the energy release scales linearly with the mass transfer rate. The ratios of predicted energy release from the particle model to the total energy release throughout the grid found hydrodynamically are 0.73, 1.1, and 1.1 for the three transfer rates considered, in order of increasing mass transfer.

The overall agreement between the particle model and the hydrodynamic calculations seems quite good through the short period of time covered by the calculations. This is to be expected since basically similar physics are employed in each calculation. The hydrodynamic calculations indicate that radiative energy dissipation in shock fronts is a mechanism capable of rapidly transforming the gas into circular motion. Furthermore, these calculations provide a size and temperature for the spot, quantities not obtainable from particle trajectory considerations. Had sufficient funds been available to extend the calculations for, say,

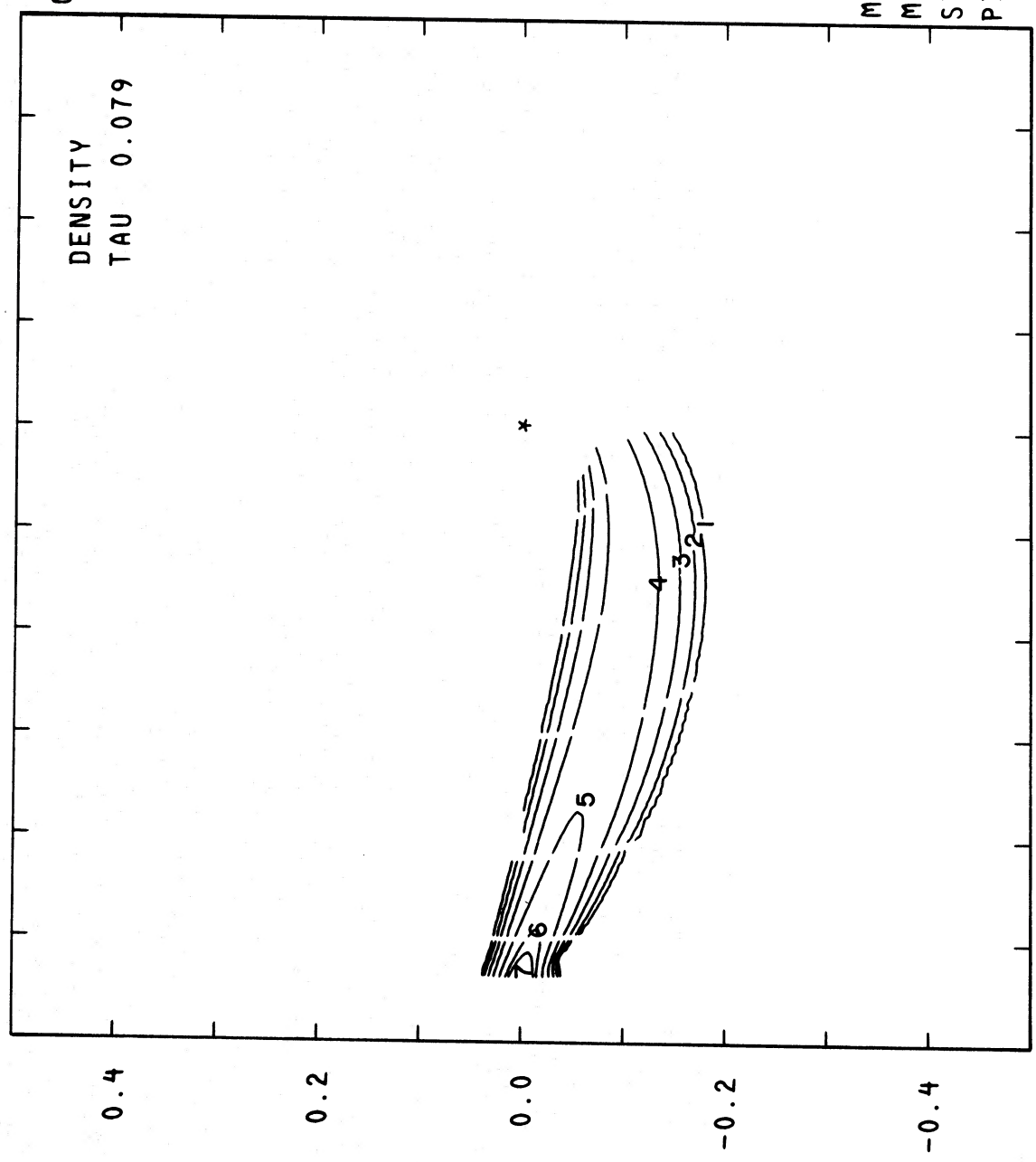

FIG. 22.—Column density contours for the stream from L_1 calculated with higher resolution than in the grid representing the complete Roche lobe

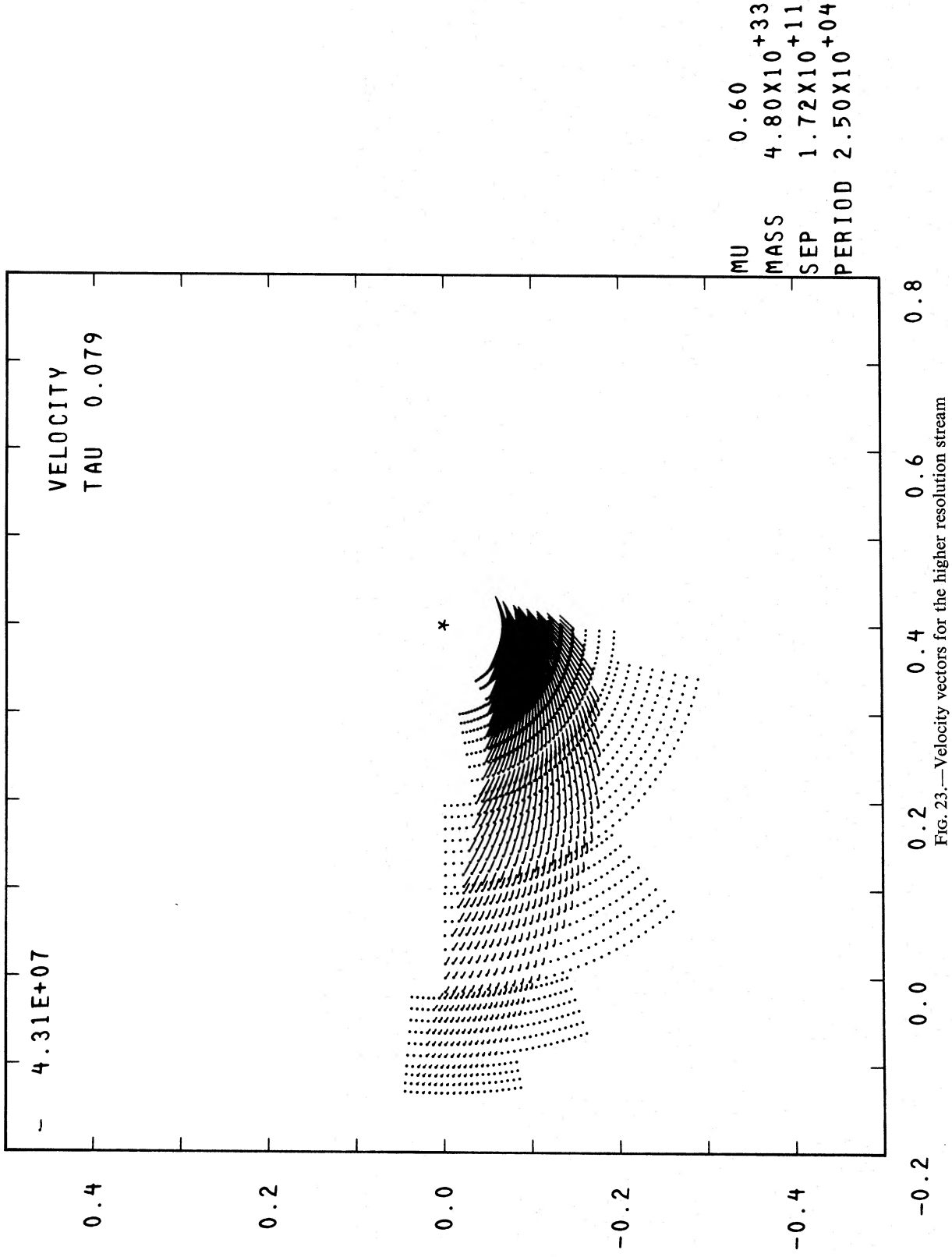

FIG. 23.—Velocity vectors for the higher resolution stream

one or two orbital periods at each mass transfer rate, it is possible that nearly complete agreement with the particle model would have been obtained in every case.

VI. SUMMARY AND DISCUSSION OF THE RESULTS

In the context of a binary star mass transfer calculation, the hydrodynamic results described above indicate that ring formation is rapid and straightforward in a system in which the transfer occurs without immediate interaction with the star receiving mass. The formation of a shock along the interface between the relatively more dense gas flowing from L_1 and the gas returning after circuiting the star rapidly drains energy from the gas via radiative cooling. The less energetic gas settles into a dense ring at a radius appropriate to its angular momentum. Within only one-third of an orbital period the ring is of sufficient density to completely impede the stream's progress, and a hot spot forms at the intersection of stream and ring. Similar results should be expected in any system meeting the criteria of (1) a star small enough to intercept only a small fraction of the stream from the component losing mass; and (2) mass ejection at relatively low velocity and reasonably confined to the orbital plane. Prendergast and Taam's calculation in which condition (1) was not satisfied indicates the difficulty of quick ring formation when the stream strongly interacts with a stellar atmosphere. In binary X-ray stars where condition (1) is almost certainly satisfied, it is likely that condition (2) is not, and a much more confused flow is likely. The presumably inevitable transformation from ring to disk cannot be followed by the numerical procedure used here. The works of Prendergast and Burbidge (1968), Lynden-Bell (1969), and Pringle and Rees (1972) address this topic (in a one-body system). The mechanism of ring dissipation is thought to be turbulent viscosity acting over a length scale of the order of or smaller than the disk thickness. Both the time scale for disk formation and the length scale for viscous interaction are incompatible with the scheme used here; the first is too long and the second too short.

The hydrodynamic results confirm the major proposed elements of the hot-spot model. They indicate the rapid formation of an optically thick, relatively confined shock with roughly the correct temperature, luminosity, and location to satisfy the observed properties of CV stars attributed to the hot spot. Some additional details of the calculation suggest explanations for two other common features of CV stars. First, the relatively rapid response of the model's total luminosity, most of which arises in the spot, to the reduced mass transfer rate indicates that a modulation in the mass transfer rate can produce flickering, as has been suggested in many earlier studies. The actual response time of 4 minutes to produce 70 percent light variation is longer than might actually be expected. The spot's radiative cooling time is only about 30–40 s, but the density gradient is blurred by the numerical calculation. Second, the observed separation between the peaks of double emission lines indicates that they are formed in gas orbiting at a radius which fills or exceeds the white dwarf's Roche lobe in a circular Keplerian approximation. The double lines are also secularly variable in intensity and separation. For example, in Z Cam the Keplerian radius from the emission lines peaks is $r/a = 0.55$ (Robinson 1973*b*), and the line separation is variable (Kraft *et al.* 1969). Frequently the emission lines in Z Cam are not even resolvable as double. The hydrodynamic results produce individually transient, low-density gaseous material which spins off the disk and proceeds farther into the Roche lobe. The observed gas producing the double emission lines must be of low density or the spot could not form so deep inside the disk. Probably the observed gas is visible as a result of radiative heating by ionizing photons from the hot spot or white dwarf. The calculated gaseous excursions become more frequent and extend farther into the Roche lobe as the grid responds to the variation in mass transfer rate. The calculations indicate that both the flickering and the low-density gaseous disk are associated with a modulated mass transfer rate. Of course, these results shed no light on the source of the modulation.

The hydrodynamic results pertaining to the spot's location are in accord with particle trajectory models for the same mass fraction. However, the derived radius to the spot should be regarded as a lower limit in practice. If the disk were to shrink, the injection of angular momentum by the stream would soon reestablish the radius found here. But viscous development of the disk would cause broadening outward as well as inward. In fact, Krzemiński and Smak found the spot's radius in WZ Sge to vary by 25 percent of a time scale of days. The variation of emission-line profiles similarly indicates a complex behavior in the actual stars. The discussion of Flannery (1975) points out that the simple spot-disk configuration of the particle trajectory models does not account for the observed phasing of eclipses and hump visibility in CV stars.

The size of the spot found here, 30°, is apparently much larger than the values of 5°–10° indicated observationally. The observed spot size is deduced from the duration of ingress and egress during eclipses and from the total phase of visibility of the hump during an orbital period. However, the presence of gas, particularly outside the radius to the hot spot, could seriously alter interpretations based on an opaque, circular, sharp-edged disk. Obviously the ambient gas is an important source of obscuration since the hump does disappear for roughly half the period. Foreshortening of the spot during eclipse would produce relatively rapid eclipses. It is of course possible that artificial broadening of the stream is more important than indicated by the test case.

The ultimate state of the stream and disk are not well represented by these calculations which indeed have not reached a steady state even under the approximations used here. Viscous dissipation of the ring will alter the disk's appearance by inward and outward broadening. The disk must eventually extend

inward to the stellar surface. However, the stream from L_1 plays an important role in the outer parts of the disk. Gas outside the spot radius must encounter the stream during each cycle around the star and either pass over it or be swept back into the dense inner disk. Thus there is strong reason to believe that the outer regions of the disk are of low density and quite variable in behavior.

The thrust of the preceding discussion is that while the hydrodynamic calculations have confirmed the existence of the major elements of the hot-spot model, thereby accounting for the gaseous features observed in CV stars, the diagnostic value of the model is minimal in providing additional information concerning the binary system. From the spot's location the mass fraction can be deduced using the particle models, but the observed parameters from which the location might be derived are variable. Knowledge of the spot's luminosity and system parameters—i.e., total mass, binary separation, and relative stellar masses—allows a determination of the mass transfer rate. Here the model is of use provided the system parameters can be found.

Finally, as regards the detailed results it must be emphasized that the assumptions used in performing the calculations were adopted for the expedient purpose of rendering feasible a difficult numerical calculation. Their adoption has allowed for the explicit consideration of hydrodynamic and radiative effects in a, hopefully, reasonable fashion. However, the neglect of ionization and the assumption of isothermality and hydrostatic equilibrium in the z direction can certainly cause factors of two errors in the temperature determination. Therefore, comparisons are best left on the general level of the preceding discussion.

VII. CONCLUSIONS

A numerical method for simulation of gas flow in binary stars has been described and applied to study mass transfer in a system scaled to resemble the dwarf nova Z Cam. The procedure reduces the problem to two-dimensional, time-dependent flow in a cylindrical Eulerian grid explicitly including gravitational and pressure forces and allowing for radiative cooling and shock formation. Unfortunately, the approximations required to produce a tractable problem also result in solutions which cannot be regarded as models for particular systems. Furthermore, the gas flow can only be followed for a short length of time, measurable in orbital periods, before the cost becomes prohibitive.

Nonetheless, the calculations presented here have produced several general results which seem valid in spite of the approximations. With the inclusion of hydrodynamic effects it is found that ring formation around the star receiving mass occurs rapidly in systems where the transfer proceeds from low-velocity mass transfer confined to the orbital plane, and in which the star does not immediately intercept the gas flow. The hydrodynamic calculations also confirm the existence of the major elements of the hot-spot model proposed to account for observed features of CV stars at minimum light. However, the observed variability of the gaseous features in CV stars makes it difficult to apply the model results accurately enough to obtain additional interpretive information with confidence.

I am grateful to William Mathews, Peter Bodenheimer, and Ronald Taam for useful suggestions and criticisms regarding the computational procedures described here, to Edward L. Robinson for many stimulating discussions regarding the observations and interpretations of cataclysmic variable stars, and especially to my advisor John Faulkner for encouragement and support during this investigation.

Parts of this study were funded by National Science Foundation grant GP-32337X. I would like to acknowledge support from an IBM Predoctoral Fellowship during parts of this investigation.

APPENDIX

OPTICALLY THIN COOLING

As pointed out in the text, in low-density or low-temperature regions of the gas flow, the gas will be optically thin through the disk. This appendix derives optically thin cooling times to show that even for optically thin cooling, the low-density gas considered here will probably not heat appreciably. From the integrated cooling function, $\Lambda(X, T)$, of Dalgarno and McCray (1972), the emission coefficient is

$$j = n_{\rm H}{}^2 \Lambda(X, T) \text{ ergs cm}^{-3} \text{ s}^{-1} . \tag{A1}$$

The cooling function was derived for a Population I composition gas in thermodynamic equilibrium at temperature T, and with degree of ionization $X = n_e/n_{\rm H}$. With the assumption that X, as well as T, is constant with z, and with the density distribution of equation (11), the integrated flux through the disk can be explicitly evaluated as an integral of $n_{\rm H}{}^2$ over all z,

$$F = \Lambda(X, T)\left[\frac{\rho_0}{\mu_{\rm H} M_{\rm H}}\right]^2 \int_{-\infty}^{\infty} \exp\left[-2(z/L)^2\right] dz \text{ ergs cm}^{-2} \text{ s}^{-1} , \tag{A2}$$

TABLE A1

OPTICALLY THIN COOLING

		σt_c (s g cm^{-2}) × 10^4			
		R_{10}			
T_4	X	1	2	5	10
0.5.....	10^{-4}	110	300	1200	3500
0.5.....	0.03	2.2	6.1	24	70
1.0.....	1	0.9	2.6	10	30
2.0.....	1	0.1	0.4	1.5	4
10.0.....	1	0.5	1.3	5.2	15

where μ_H and M_H are the mean atomic weight per H atom and the proton mass, respectively. In terms of the column density, $\sigma = \rho_0 L\pi^{1/2}$, the integrated loss rate is

$$F = \frac{1}{[\mu_H M_H]^2 2\pi^{1/2}} \frac{\sigma^2 \Lambda(X, T)}{(T^*/A)^{1/2}} \text{ ergs cm}^{-2}\text{ s}^{-1}. \tag{A3}$$

From the total thermal content of the gas, $2\sigma T^*$, the cooling time appropriate to equation (A1) can be evaluated. If A, equation (10), is approximated as GM/r^3, and units of 10^4 K (T_4), solar masses (M), 10^{10} cm (R_{10}), and 10^{-22} ergs cm^3 s^{-1} (Λ_{-22}) are used, then the product of column density and cooling time can be expressed as

$$\sigma t_c = 9 \times 10^{-6} \frac{[R_{10} T_4]^{3/2}}{M^{1/2}} \frac{1}{\Lambda_{-22}} \text{ s g cm}^{-2}. \tag{A4}$$

The resultant cooling times are tabulated in Table A1 for a range of temperatures and radii. For temperatures greater than 10^4 K the cooling function is large enough that cooling times for densities greater than the cutoff density, 10^{-4} g cm^{-2}, are in the range of 0.1–30 s. Below 10^4 K the cooling function depends strongly on the degree of ionization, which is not calculated here. Quite long cooling times are possible if the ionization falls to 10^{-4} at temperatures lower than about 5×10^3 K. In summary, even optically thin cooling seems efficient enough to prevent the gas considered in this problem from heating appreciably under the influence of purely mechanical heating.

REFERENCES

Batten, A. 1970, *Pub. A.S.P.*, **82**, 574.
Biermann, P. 1971, *Astr. and Ap.*, **10**, 205.
Dalgarno, A., and McCray, R. 1972, *Ann. Rev. Astr. and Ap.*, **10**, 375.
Faulkner, J. 1974, in *IAU Symposium No. 66, Late Stages of Stellar Evolution*, ed. R. J. Tayler and J. E. Hesser (Dordrecht: Reidel), p. 155.
Flannery, B. P. 1975, *M.N.R.A.S.*, **170**, 325.
Gould, N. 1957, *Pub. A.S.P.*, **69**, 541.
———. 1959, *A.J.*, **64**, 136.
Kopal, Z. 1956, *Ann. d'Ap.*, **19**, 298.
Kraft, R. 1963, *Adv. Astr. and Ap.*, **2**, 43.
Kraft, R., Krzemiński, W., and Mumford, G. 1969, *Ap. J.*, **158**, 589.
Kruszewski, A. 1964, *Acta Astr.*, **14**, 231.
Krzemiński, W. 1965, *Ap. J.*, **142**, 1051.
Krzemiński, W., and Smak, J. 1971, *Acta Astr.*, **21**, 133.
Kuiper, G. 1941, *Ap. J.*, **93**, 133.
Lynden-Bell, D. 1969, *Nature*, **233**, 690.
Mumford, G. 1967, *Pub. A.S.P.*, **79**, 283.
Paczynski, B. 1971, *Ann. Rev. Astr. and Ap.*, **9**, 183.
Plavec, M. 1968, *Adv. Astr. and Ap.*, **6**, 201.
Prendergast, K. 1960, *Ap. J.*, **132**, 162.
Prendergast, K., and Burbidge, G. 1968, *Ap. J. (Letters)*, **151**, L83.
Prendergast, K., and Taam, R. 1974, *Ap. J.*, **189**, 125.
Pringle, J., and Rees, M. 1972, *Astr. and Ap.*, **21**, 1.
Robinson, E. 1973*a*, *Ap. J.*, **180**, 121.
———. 1973*b*, *ibid.*, **186**, 374.
Sanders, R., and Prendergast, K. 1974, *Ap. J.*, **188**, 489.
Warner, B., and Nather, R. 1971, *M.N.R.A.S.*, **152**, 219.
———. 1972*a*, *ibid.*, **156**, 297.
———. 1972*b*, *ibid.*, p. 305.
Warner, B., and Peters, W. 1972, *M.N.R.A.S.*, **160**, 15.

BRIAN P. FLANNERY: Lick Observatory, University of California, Santa Cruz, CA 95064